Cell

Encoding and Transducing the Synaptic or Extrasynaptic Origin of NMDA Receptor Signals to the Nucleus

Anna Karpova,[1,7] Marina Mikhaylova,[1,4,7] Sujoy Bera,[1] Julia Bär,[1] Pasham Parameshwar Reddy,[1] Thomas Behnisch,[5] Vladan Rankovic,[1] Christina Spilker,[1] Philipp Bethge,[1,8] Jale Sahin,[1,9] Rahul Kaushik,[1] Werner Zuschratter,[2] Thilo Kähne,[6] Michael Naumann,[6] Eckart D. Gundelfinger,[3] and Michael R. Kreutz[1,*]

[1]RG Neuroplasticity

[2]Special Lab Electron and Laserscanning Microscopy

[3]Department of Neurochemistry and Molecular Biology

Leibniz Institute for Neurobiology, 39118 Magdeburg, Germany

[4]Cell Biology, Faculty of Science, Utrecht University, 3584 CH Utrecht, the Netherlands

[5]Institutes of Brain Science and State Key Laboratory of Medical Neurobiology, Fudan University, Shanghai 200032, People's Republic of China

[6]Institute of Experimental Internal Medicine, Otto-von-Guericke University Magdeburg, 39120 Magdeburg, Germany

[7]These authors contributed equally to this work

[8]Present address: CNRS, Interdisciplinary Institute for Neuroscience, UMR 5297, 33000 Bordeaux, France

[9]Present address: National Metrology Institute, TÜBITAK-UME, 41470 PK 54 Kocaeli, Turkey

*Correspondence: kreutz@lin-magdeburg.de

http://dx.doi.org/10.1016/j.cell.2013.02.002

SUMMARY

The activation of N-methyl-D-aspartate-receptors (NMDARs) in synapses provides plasticity and cell survival signals, whereas NMDARs residing in the neuronal membrane outside synapses trigger neurodegeneration. At present, it is unclear how these opposing signals are transduced to and discriminated by the nucleus. In this study, we demonstrate that Jacob is a protein messenger that encodes the origin of synaptic versus extrasynaptic NMDAR signals and delivers them to the nucleus. Exclusively synaptic, but not extrasynaptic, NMDAR activation induces phosphorylation of Jacob at serine-180 by ERK1/2. Long-distance trafficking of Jacob from synaptic, but not extrasynaptic, sites depends on ERK activity, and association with fragments of the intermediate filament α-internexin hinders dephosphorylation of the Jacob/ERK complex during nuclear transit. In the nucleus, the phosphorylation state of Jacob determines whether it induces cell death or promotes cell survival and enhances synaptic plasticity.

INTRODUCTION

N-methyl-D-aspartate-receptors (NMDARs) are heterotetrameric ligand- and voltage-gated Na^+/Ca^{2+} channels that play a pivotal role in synaptic plasticity and memory formation, as well as in cell death and survival signaling (Köhr, 2006; Hardingham and Bading, 2010). Many aspects of these diverse functions require the regulation of gene expression and, hence, synapse-to-nucleus communication. Thus, it is generally believed that synaptic activity regulates gene expression that is required for long-term changes of membrane excitability and the formation of long-term memory; the contribution of long-distance NMDAR signaling to the nucleus is essential in this regard (Alberini, 2009; Flavell and Greenberg, 2008; Jordan and Kreutz, 2009). However, NMDARs are present at synaptic and extrasynaptic sites. In recent years, it became increasingly clear that, depending upon their localization, the activation of these receptors has fundamentally different consequences with respect to nuclear gene expression (Hardingham and Bading, 2010). Whereas activation of synaptic NMDARs induces the expression of cell survival and plasticity genes, the activation of extrasynaptic NMDARs primarily drives the expression of cell death genes (Papadia et al., 2008; Zhang et al., 2007; Hardingham and Bading, 2010). The functional dichotomy of NMDAR signaling has attracted enormous interest as the extrasynaptic pathway was linked to disease states like brain ischemia, Huntington's disease, and others (Okamoto et al., 2009; Milnerwood et al., 2010; Tu et al., 2010; Zhang et al., 2011). To date, no molecular mechanisms are known that couple long-distance synaptic and extrasynaptic NMDAR signaling to gene expression or that distinguish both pathways in the nucleus (Hardingham and Bading, 2010).

Previously, we found that extrasynaptic NMDAR activation, as well as pathogenic agents (e.g., amyloid-β peptide), induces long-haul transport of the protein messenger Jacob to the nucleus, where it then induces a sustained dephosphorylation of CREB, rendering the transcription factor inactive (Dieterich et al., 2008; Rönicke et al., 2011). Overexpression of Jacob results in gene expression that elicits neurodegeneration, whereas suppression has the opposite effect (Dieterich et al.,

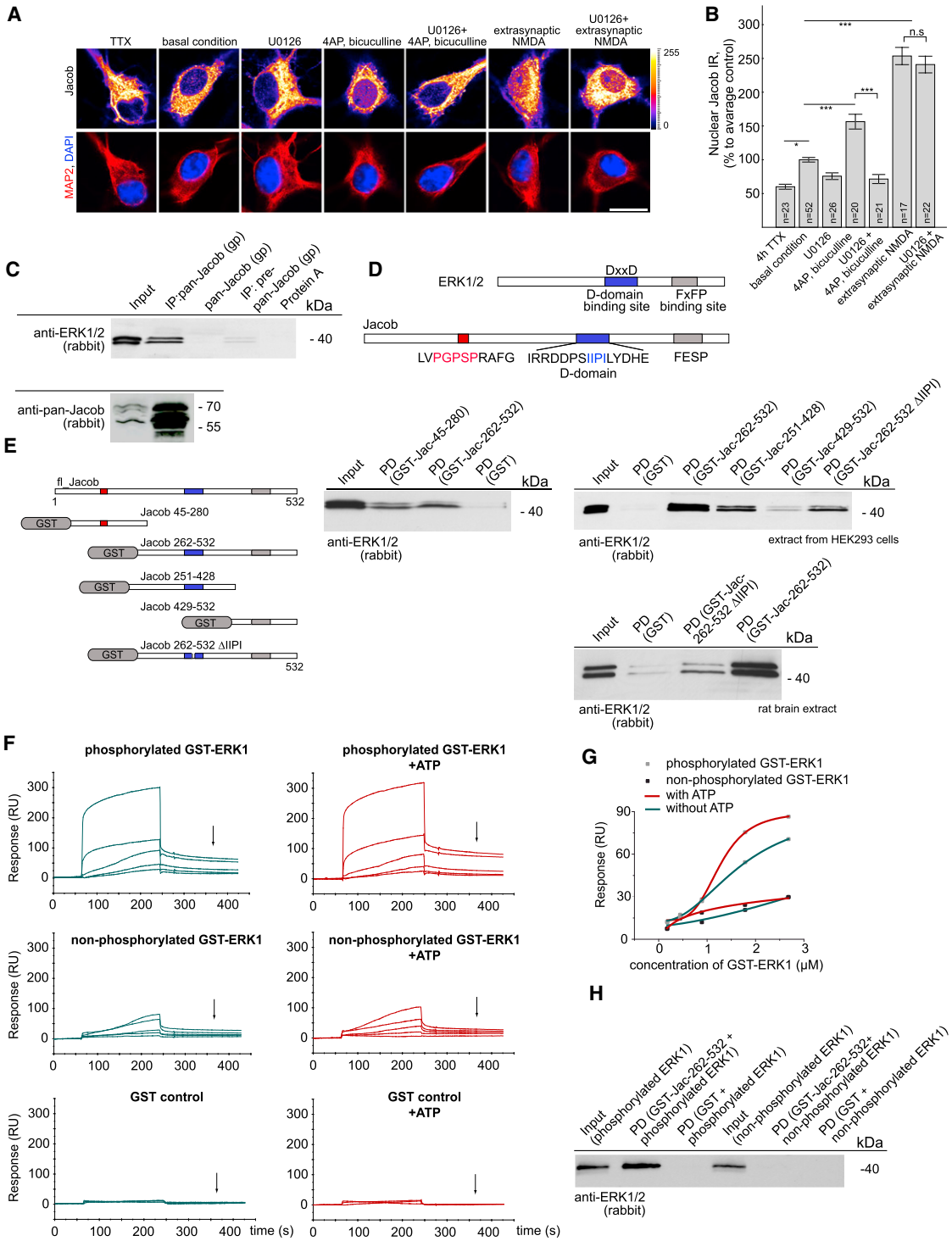

Figure 1. The Nuclear Translocation of Jacob after Activation of Synaptic NMDARs, but Not Extrasynaptic NMDARs, Requires MAP Kinase Activity and Physical Interaction of Jacob with ERK1/2

(A and B) The increase in nuclear Jacob immunoreactivity after enhanced synaptic NMDAR activity is accompanied by a higher activation level of ERK. Nuclear import of Jacob is abolished by application of the MEK inhibitor U0126 (10 μM). The presence of MEK inhibitor during extrasynaptic NMDAR stimulation does not prevent the nuclear import of Jacob. Confocal images averaged from three confocal sections of the nucleus of DIV16 hippocampal primary neurons stained for pan-Jacob (rabbit) and for the active form of ERK1/2 (pERK, mouse). Original pixel intensities from 0 to 255 are represented as a gradient lookup table. Scale bar, 10 μm. Intensity-based quantification of nuclear Jacob IR. Data are represented as mean ±SEM. ***p < 0.001, as determined by Bonferroni corrected t tests.

(legend continued on next page)

2008). Taken together, these data suggest that Jacob is a messenger of cell death in the extrasynaptic NMDAR pathway to the nucleus (Dieterich et al., 2008; Kindler et al., 2009; Rönicke et al., 2011).

However, the protein also translocates to the nucleus after stimulation of synaptic NMDARs, albeit to a lesser extent (Dieterich et al., 2008), as well as after the induction of NMDAR-dependent long-term potentiation (LTP), but not long-term depression (LTD), in CA1 neurons, suggesting that Jacob might also be involved in hippocampal LTP-dependent learning and memory processes (Behnisch et al., 2011). Given that Jacob is a messenger in both pathways, the following questions arise: how is it possible to distinguish whether the activation of extrasynaptic or synaptic NMDARs caused its nuclear import and why does this occur after the induction of NMDAR-dependent LTP, but not LTD?

Activation of the mitogen-activated protein kinase (MAPK) ERK1/2 in the hippocampus requires high-frequency stimulation of NMDARs. The induction of LTP, but not LTD, results in ERK1/2 phosphorylation (Thomas and Huganir, 2004). Most importantly, extrasynaptic NMDAR signaling has no effect on ERK1/2 phosphorylation, whereas sustained synaptic NMDAR signaling triggers the nuclear import of active ERK1/2 (Ivanov et al., 2006; Kim et al., 2005; Hardingham and Bading, 2010). Here, we show that, after sustained stimulation of synaptic NMDARs, but not of extrasynaptic NMDARs, the nuclear translocation of Jacob becomes dependent on ERK1/2 activity. Moreover, we demonstrate that Jacob is an ERK-binding protein that is phosphorylated by ERK1 at serine 180 after enhanced activation of synaptic NMDARs. Binding of the neurofilament α-internexin forms a stable trimeric complex that hinders the dephosphorylation of Jacob and ERK during long-distance transport. We show that NMDAR-dependent LTP, but not LTD, increases Ser180 phosphorylation and that the nuclear overexpression of a phosphomimetic Jacob mutant leads to gene expression and subsequent morphological and electrophysiological changes characteristic of enhanced synaptic strength. The presence of nonphosphorylated Jacob in the nucleus has the opposite effect and is followed by a series of deteriorative events in terms of synaptic integrity that subsequently cause cell death. In summary, Ser180 phosphorylation of Jacob by ERK encodes the synaptic versus extrasynaptic localization of NMDARs, thus providing the first mechanism to distinguish these pathways in the nucleus.

RESULTS

ERK Activity Distinguishes the Synaptic and Extrasynaptic NMDAR-Jacob Pathways

The MAP kinase ERK1/2 are downstream effectors of synaptic NMDARs involved in NMDAR-activation-induced gene expression, whereas signaling via extrasynaptic NMDAR has no effect on ERK1/2 (Kim et al., 2005; Ivanov et al., 2006). We therefore asked whether ERK1/2 activity is required for the nuclear translocation of Jacob after synaptic NMDAR stimulation. Intriguingly, we found that U0126, a MEK1/2 inhibitor, blocks the nuclear accumulation of Jacob after selective stimulation of synaptic NMDARs, but not of extrasynaptic NMDARs (Figures 1A and 1B).

Jacob Directly Associates with ERK and Is an ERK Substrate

Coimmunoprecipitation experiments confirmed that Jacob and ERK1/2 form a complex in vivo (Figure 1C). Jacob harbors a potential ERK phosphorylation site at serine 180 and has two potential ERK-binding domains at amino acids 367–382 and 487–501 (Figure 1D and Figure S1A available online). To learn how Jacob associates with ERK, we performed pull-down assays using recombinant GST-Jacob and HEK293 cell or rat brain extracts. In these experiments, endogenous ERK1/2 were pulled down with both the N- and C-terminal halves of Jacob (Figure 1E). Binding was much weaker to a fusion protein lacking four amino acids in the first ERK-binding domain (Jacob-ΔIIPI lacking the D domain) or to a fusion protein harboring only the FESP motif (Figures 1D and 1E), suggesting that the D domain might have the highest affinity for binding.

We next analyzed the interaction in quantitative terms employing surface plasmon resonance (SPR). We coupled recombinant 6xHis-SUMO-Jacob-Δ1-44 to the surface of a sensor chip and injected phosphorylated and nonphosphorylated GST-ERK1 fusion proteins. Although a GST-control protein did not bind to

(C) Coimmunoprecipitation of Jacob and ERK1/2 from a soluble rat brain protein fraction. Immunoprecipitation (IP) with a pan-Jacob guinea pig antibody. Two bands are visible in the precipitate that correspond to ERK1 and 2. ERK1/2 were only found in the IP with the Jacob antibody, whereas they remained in the supernatant of a preimmune serum IgG, a pan-Jacob antibody IP control without brain extract, and a Protein A sepharose control. Lower panel shows the efficiency of immunoprecipitation.

(D) Two predicted docking sites at the C terminus of Jacob identified by sequence homology to other ERK1/2 substrate binding motifs (D domain, blue box; FXFP docking site, gray box).

(E) Cartoon depicting GST-Jacob constructs used for the pull-down assays. Both the N and C termini of Jacob bind to ERK1/2 from HEK293 cell extracts in GST pull-down assay (middle). Deletion of the IIPI motif (D domain) reduces Jacob-ERK1/2 binding (right). A weak interaction was observed between ERK and the C terminus of Jacob that contains only the FxSP motif (right). Similar results were obtained in pull-down assays using a rat brain extract (bottom).

(F) SPR studies confirm the direct interaction between 6xHis-SUMO-Jacob-Δ1-44 and ERK1. The presence of ATP in the analyte enhances binding of phosphorylated ERK1 to Jacob. 6xHis-SUMO-Jacob-Δ1-44 was immobilized on the sensor chip, and phosphorylated GST-ERK1, nonphosphorylated GST-ERK1, and GST controls were added as analyte. Assays were carried out in the presence or absence of adenosine triphosphate (Mg^{2+}-ATP; 30 μM). Sensorgrams were processed by blank subtraction showing the net increase in amplitudes. Maximal response units in the dissociation phase for different concentrations were plotted (indicated by an arrow) and used to compare different conditions.

(G) Saturation of binding plotted from the dissociation phase of the interaction indicates higher affinity binding for phosphorylated ERK1 as compared to the nonphosphorylated kinase.

(H) GST pull-down assays using bacterially expressed GST-Jacob-262-532 and recombinant ERK1. The matrix-coupled GST-Jacob fusion protein efficiently pulls down phosphorylated ERK1, but not nonphosphorylated ERK1.

See also Figure S1.

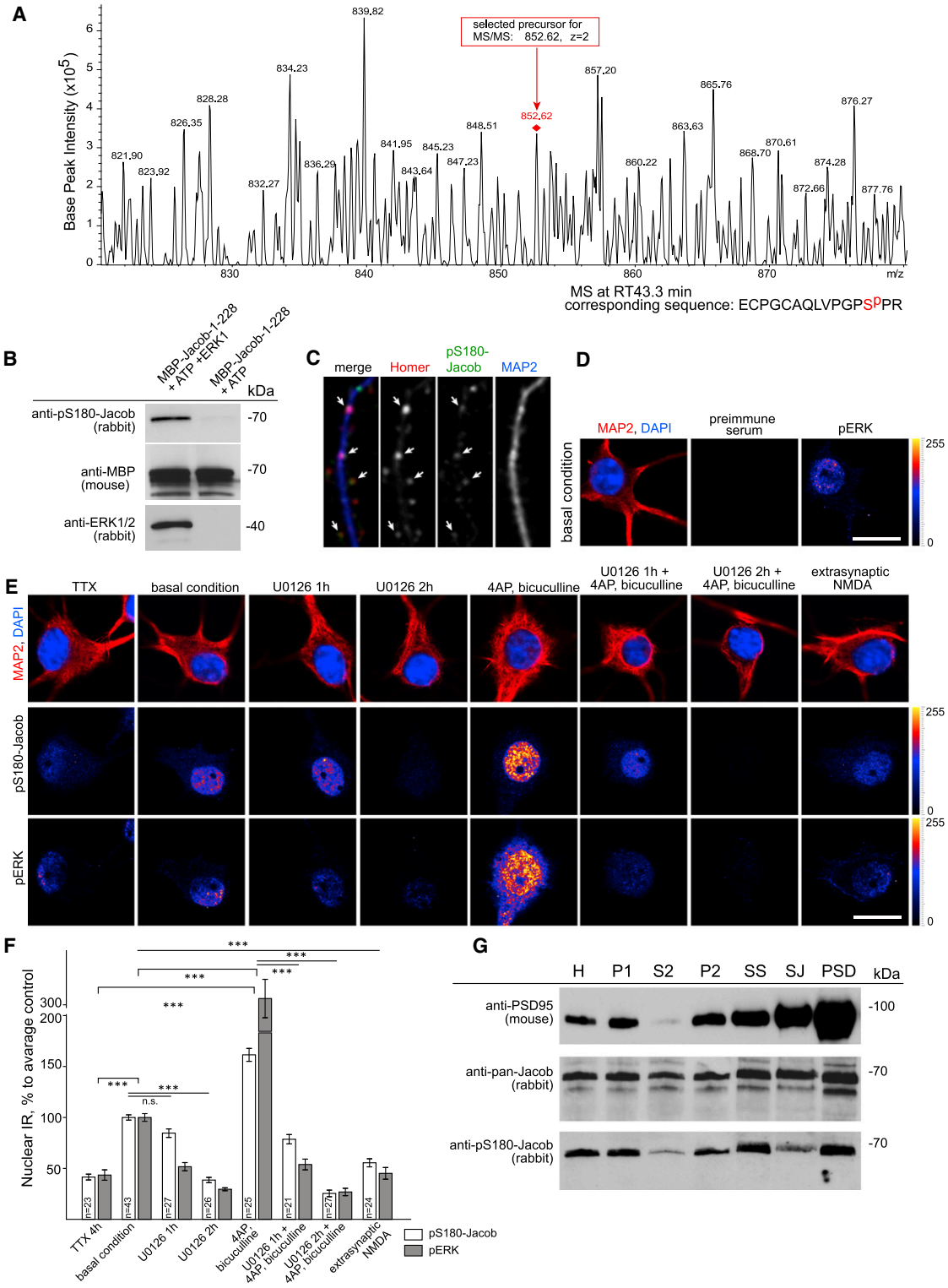

Figure 2. Jacob Is an ERK1 Substrate In Vitro and In Vivo

(A) ERK phosphorylates Jacob in 18DIV cortical primary neurons treated with 50 μM bicuculline/2.5 mM 4-AP. Nuclear extracts from WT-Jacob-GFP-infected neurons were separated in duplicate by SDS-PAGE. One lane from each sample was processed for immunoblotting with GFP and pS180-Jacob antibody, and a second one was stained with Coomassie blue. The area corresponding to the band of WT-Jacob-GFP was cut out from the SDS gel and underwent InGel digestion. Resulting peptides were subjected to a nanoreversed phase (C18)-HPLC online coupled to an ETDII iontrap mass spectrometer. Tandem mass

(legend continued on next page)

immobilized Jacob, we found a specific and saturable binding of GST-ERK1 (Figure 1F). Moreover, we observed that binding to Jacob is dependent upon ERK activity. Nonphosphorylated ERK1 associated to a much lower extent than phosphorylated ERK1, as determined from the dissociation phase of the interaction (Figures 1F and 1G). A further increase in response was seen when we added ATP, conditions which promote the phosphorylation of Jacob by ERK1 (Figure 1F). In addition, a GST-Jacob fusion protein interacts more efficiently with active versus inactive ERK1 (Figure 1H).

Next, we directly assessed whether Ser180 is an ERK phosphorylation site. An in vitro ERK kinase assay and subsequent nano-LC-ESI-MS/MS analysis demonstrated the incorporation of a phosphate at position 180 in a bacterially expressed 6-His-SUMO-Jacob-Δ1-44 fusion protein (Figures S1A and S2A). No other phosphorylation site was identified in this assay (Figure S2A). In addition, this phosphorylation site is highly conserved in different mammalian species (except mouse, see Supplemental Information and Figures S1B–S1F). Moreover, we found that, after viral expression of WT-Jacob-GFP in primary cortical neurons, Jacob is phosphorylated at serine 180 in vivo (Figure 2A).

Ser180 Phosphorylation Is Induced by Synaptic Activity

To further explore the role of phosphorylation at this site, we generated a phosphospecific antibody (pS180-Jacob; see Extended Experimental Procedures and Figures 2B–2E and S2B–S2H). The antibody detects phospho-S180 in an MBP-Jacob-1-228 fusion protein preincubated with active ERK1 and ATP, but not the nonphosphorylated Jacob (Figure 2B). Immunocytochemical staining revealed prominent pS180-Jacob immunofluorescence in the nucleus and synapses and, to a lesser extent, in dendrites (Figures 2C–2E). Moreover, pS180-Jacob immunoreactivity (IR) was detected in the postsynaptic density fraction (PSD) in subcellular fractionation experiments (Figure 2G). We next asked whether synaptic and extrasynaptic NMDAR stimulation might differentially regulate the phosphorylation of Jacob. Only in the first case did we find an increased nuclear pS180-Jacob immunofluorescence, whereas extrasynaptic NMDAR stimulation had the opposite effect (Figures 2E and 2F). The increase in staining intensity was blocked when, concomitant to enhancing synaptic activity, the MEK inhibitor U0126 was applied (Figures 2E and 2F). Interestingly, nuclear overexpression of myristoylation-deficient Jacob-ΔIIPI, lacking the high-affinity ERK docking site, showed no enhancement of pS180-Jacob immunostaining as compared to the corresponding myristoylation mutant containing this binding motif (Figure S2E). Scansite 2.0 suggests that Ser180 might also be phosphorylated by cyclin-dependent kinase 5 (CDK5). However, administration of the CDK5 inhibitor roscovitine had no effect on pS180 immunofluorescence (Figures S2F–S2H), suggesting that Ser180 is most likely a specific ERK phosphorylation site in vivo.

Jacob Translocates from Synapses to the Nucleus in an ERK-Dependent Manner

For any molecule to be considered a true synapto-nuclear messenger, a minimum requirement is an activity-dependent dissociation from synaptic sites, which correlates with an increase in nuclear protein levels. Because the latter was previously shown (Dieterich et al., 2008; Kindler et al., 2009), we increased network activity and synaptic glutamate release with bicuculline and applied quantitative immunocytochemistry to study the synaptic association of Jacob. As shown in Figure S3, the immunofluorescence of synaptic Jacob was indeed significantly reduced within 10 min following bicuculline application, as compared to tetrodotoxin (TTX)-treated control neurons (Figures S3A and S3B). Most importantly, high-frequency field stimulation (18 s/50 Hz), which induces LTP in hippocampal primary neurons (Deisseroth et al., 1996), leads to a pronounced and rapid dissociation of WT-Jacob-GFP from dendritic spines (Figures 3A and 3B). Further evidence that Jacob rapidly dissociates from synaptic sites in an activity- and ERK-dependent manner was obtained when we expressed full-length Jacob-GFP in primary neurons using a Semliki-Forest virus (Figures S3C and S3D). After stimulation of synaptic NMDARs, WT-Jacob-GFP rapidly moved out of dendritic spines (Figures S3C and S3D), whereas it was retained in dendritic spines following stimulation when we preincubated the culture with the MEK-inhibitor U0126 (Figure 3D). We then generated a phosphodeficient mutant by replacing Ser180 with alanine (S180A- Jacob-GFP). DIV25-27 neurons were transfected with WT-Jacob-GFP

spectrometry (MS/MS) precursor selection was tuned for the preferential use of masses corresponding to a double-charged (852.36 Da) putative ECPGCAQLVPGPSPPR Jacob peptide. Depicted is the mass spectrum at retention time 43.3 min, including the 852.62 Da double-charged base peak peptide, which was selected as a precursor for two independent collision-induced dissociation (CID) fragmentations. Both MS/MS experiments significantly revealed sequence identity of the selected precursor to the phosphorylated ECPGCAQLVPGPSpPR sequence of Jacob.

(B) The anti-pS180-Jacob antibody recognizes phosphorylated Jacob, but not nonphosphorylated Jacob. Recombinant active ERK1 was used to phosphorylate bacterially expressed MBP-Jacob-1-228 at Ser180 in the presence of ATP. Anti-MBP antibody staining shows that equal amounts of protein were used in both reactions.

(C) A representative confocal image of dendritic segment stained with an anti-MAP2 antibody (blue) is depicted. Arrows indicate pS180-Jacob spots at a subset of excitatory synapses as demonstrated by double-immunofluorescence staining with an anti-Homer antibody (red).

(D) The pS180 Jacob preimmune serum shows no nuclear staining. Scale bar, 20 μm.

(E and F) Enhanced synaptic activity increases nuclear pS180-Jacob IR. The increase is abolished in the presence of 10 μM U0126. In contrast, stimulation of extrasynaptic NMDARs results in a decrease of nuclear pS180-Jacob IR. Scale bar, 20 μm. Data are represented as mean ±SEM. ***$p < 0.001$, as determined by Bonferroni corrected t tests.

(G) Subcellular fractionation of rat brain. A 70 kDa pS180-Jacob band is present in the PSD fraction. Please note that Jacob is alternatively spliced, which results in multiple bands on western blots (Dieterich et al., 2008; Kindler et al., 2009). Low-molecular-weight pS180-Jacob bands are only visible at long exposure times. 20 μg of protein was loaded in each lane. H, homogenate; P1, crude nuclear fraction; S2, supernatant after centrifugation at 12,000 x *g*; P2, pellet fraction generated after centrifugation of precleaned homogenate at 12,000 x *g*; SS, synaptosomes; SJ, synaptic junctions; and PSD, postsynaptic density fraction. See also Figures S1 and S2.

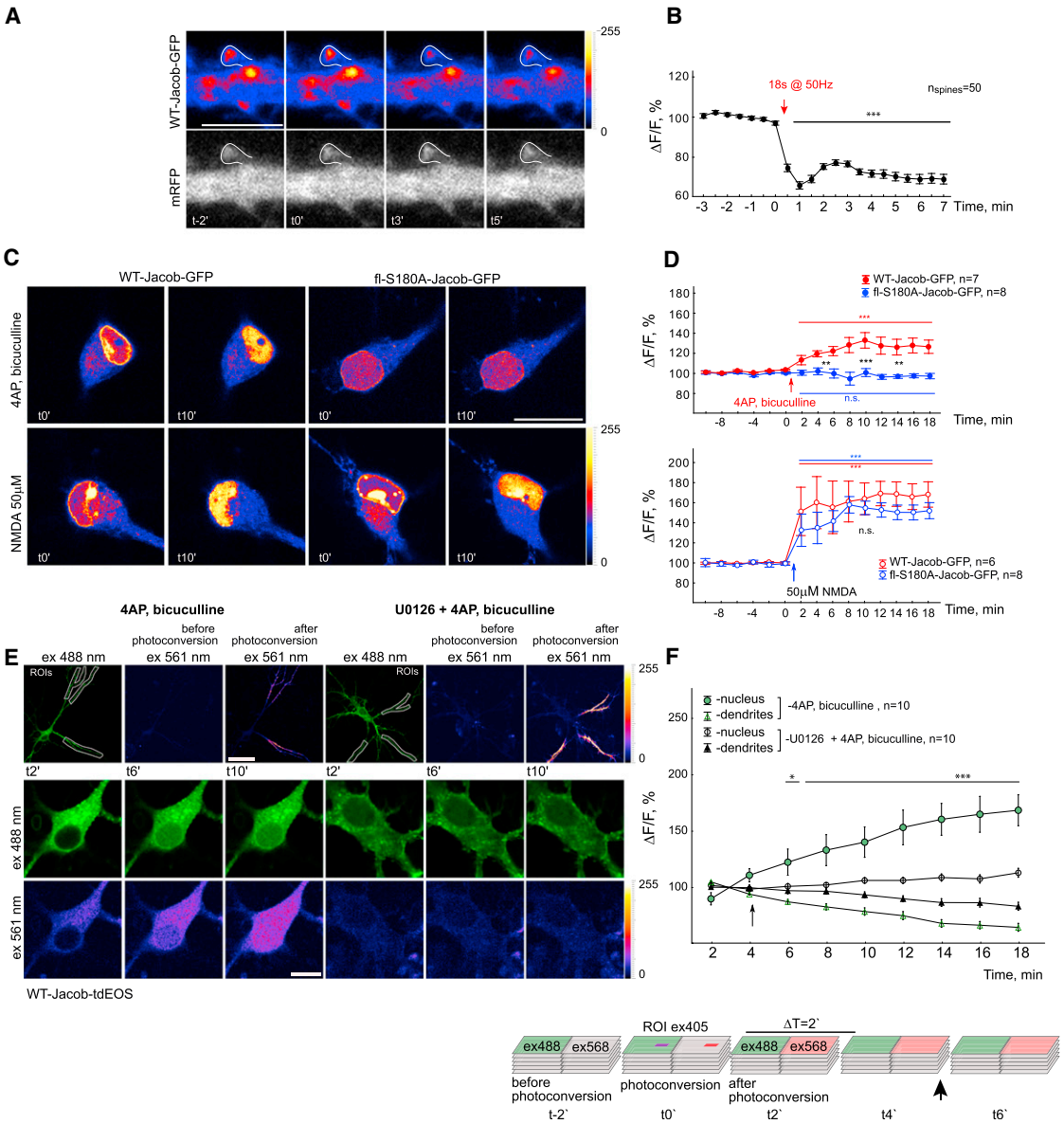

Figure 3. Synaptic Stimulation Drives Jacob from Distal Dendrites into the Nucleus in an ERK-Dependent Manner

(A and B) High-frequency field stimulation (50 Hz pulses for 18 s, 1 ms current pulse duration) results in a rapid and prominent dissociation of WT-Jacob-GFP from dendritic spines. Coexpression of mRFP served as a volume control. Depicted are representative confocal frames before (t-2′, t0′) and after (t3′, t5′) synaptic stimulation. Scale bar, 5 μm.

(C and D) Time-lapse imaging reveals that the translocation of Jacob from distal dendrites to the nucleus depends upon Ser180 phosphorylation following stimulation of synaptic NMDARs, but not extrasynaptic NMDARs. Confocal average intensity images of hippocampal neurons at DIV16/17 expressing WT-Jacob-GFP or Jacob-S180A-GFP are shown before (t0′) and after (t10′) stimulation. Scale bar, 25 μm. Nuclear Jacob-S180A-GFP (blue circles) and WT-Jacob-GFP (red circles) fluorescence intensities before and after 4-AP, bicuculline application or after bath application of 50 μM NMDA (open circles, bottom). Data are represented as mean ±SEM. ***$p < 0.001$, as determined by Bonferroni corrected t tests.

(E and F) Jacob-tdEOS was expressed in hippocampal primary neurons, and indicated regions of interest (ROIs) were illuminated with 405 nm wavelength to induce green-to-red fluorescence conversion in distal dendrites. The upper panels in (E) show effective photoconversion after illumination with 405 nm. Scale bar, 40 μm. The lower panels depict (35 × 35) μm^2 averaged frames from the nuclear plane before (t2′) and after (t6′ and t10′) synaptic stimulation. Scale bar, 10 μm. WT-Jacob-tdEOS photoconverted at distal dendrites translocates to the nucleus upon synaptic stimulation (green circles in F). At the same time, a decrease in tdEOS photoconverted fluorescence was observed at distal dendrites (F, green triangles). The presence of the MEK antagonist U0126 blocked this translocation. Data are represented as mean ±SEM. *$p < 0.05$ and ***$p < 0.001$. (F) Confocal z stacks were acquired using the xyzt-image scan mode with a 0.3 μm step size and ΔT = 2′. ROIs selected for photoconversion were illuminated with 405 nm light, and the out-of-ROI region was set to 488 nm excitation wavelength. The arrow at t4 indicates the time point of synaptic stimulation. Time points t2 and t4 were taken as baseline, and changes in pixel intensities upon bicuculline treatment were normalized to the averaged baseline.

See also Figure S3.

or the S180A mutant (Figures S3E and S3F). As expected, and in contrast to wild-type, S180A- Jacob-GFP remained at synaptic sites following enhanced synaptic NMDAR activity (Figures S3E and S3F).

We next asked whether the long-distance trafficking of Jacob to the nucleus after synaptic NMDAR activation depends upon the phosphorylation of Ser180 by ERK. Time-lapse imaging of hippocampal neurons transfected with the phosphodeficient Jacob-GFP mutant revealed that this fusion protein only accumulates in the nucleus after the activation of extrasynaptic (Figures 3C and 3D, bottom), but not synaptic, NMDARs following administration of 4-AP and bicuculline (Figures 3C and 3D, top). Further evidence for ERK-dependent Ser180 phosphorylation as a prerequisite for long-distance trafficking in response to synaptic NMDAR stimulation came from experiments where we transfected primary hippocampal neurons with a photoconvertible WT-Jacob-tdEos construct that allows the conversion of green to red fluorescence in more distal dendrites, including spines (Figures 3E and 3F). Following bath application of bicuculline, we observed a rapid increase in the nuclear red fluorescence signal within minutes, indicating dendrite-to-nucleus trafficking (Figures 3E and 3F). In stark contrast, the WT-Jacob-tdEos fusion protein remained largely stationary in dendrites when we repeated this experiment in the presence of the MEK inhibitor U0126 (Figures 3E and 3F), indicating that Ser180 phosphorylation and ERK activity are indeed necessary for long-distance synapse to nucleus trafficking.

Binding to α-Internexin Protects Phosphorylated Jacob against Phosphatase Activity during Long-Distance Trafficking to the Nucleus

Taken together, these results raise the question of whether it is at all conceivable that Jacob can traverse a phosphatase-rich environment and preserve its phosphorylation status for long-distance synapto-nuclear signaling. A plausible mechanism for the conservation of posttranslational modifications for long-distance transport was suggested by Perlson et al. (2005), who demonstrated that retrograde transport of ERK1/2 in axons requires association with importin-β and the molecular motor dynein. The concomitant binding of proteolytic fragments of the intermediate filament vimentin hinders the dephosphorylation of pERK within this complex (Perlson et al., 2005, 2006). In a yeast two-hybrid screen with Jacob, we identified α-internexin as a binding partner (Figure S4A). α-Internexin is a neuronal intermediate filament and, in contrast to vimentin, is expressed in adult neurons where it replaces vimentin during neuronal development (Benson et al., 1996; Yuan et al., 2006). We found that α-internexin is present in different subcellular fractions from adult rat brain homogenates, including cytosol, nuclei, and the PSD (Figures 4A and S5A). Immunocytochemistry revealed staining in neurites, somata, and nuclei (Figures S4B, S4C, and S5B), whereas only a sparse α-internexin staining was present in dendritic spines (Figure S4B). Analogous to vimentin, we found that α-internexin is also sensitive to proteolytic cleavage by the calcium-activated protease calpain (Figure S5C).

A GST pull-down assay using recombinant full-length α-internexin and cell extracts from HEK293 cells transfected with c-*myc*-tagged Jacob confirmed the interaction between both proteins (Figure S4D). The reciprocal pull-down with GST Jac-45-280 shows binding of α-internexin from rat brain extract (Figure S4D). Neuronal importins are present in axons, dendrites, and at synapses from where they translocate to the nucleus upon NMDAR activation (Thompson et al., 2004). Importin-α can directly associate with a dynein motor (Hanz et al., 2003), and we have previously shown that long-distance transport of Jacob requires importin-α binding (Dieterich et al., 2008), suggesting that an active transport along microtubuli is responsible for the activity-dependent nuclear import of Jacob. In support of this notion, Jacob, α-internexin, ERK1/2, importin-α, and the dynein intermediate chain are all present in a soluble microsome-free cytoplasmic fraction. Additionally, α-internexin could be coimmunoprecipitated with an anti-dynein intermediate chain antibody (Figures 4A and 4B), indicating that these proteins may associate in one complex in vivo. We next mapped the binding regions of the Jacob/α-internexin interaction using the yeast two-hybrid system. We found that an N- and C-terminal binding site exists in Jacob for the interaction with α-internexin (Figure S4A). The N-terminal site encompasses Ser180, and GST-α-internexin pulled down Jacob more efficiently after enhanced ERK activity (Figure S4E). Stimulation of HEK293 cells with EGF to increase MAPK activity enhanced binding of Jacob, whereas application of the MEK inhibitor U0126 had the opposite effect (Figure S4E). Furthermore, a direct interaction between Jacob and α-internexin was confirmed with GST pull-down assays using the recombinant proteins (Figure S4G). However, no interaction was found between GST-ERK1/2 and α-internexin (Figure S4F). Finally, binding of α-internexin does not compete with ERK binding nor does it prevent phosphorylation of Jacob by ERK in in vitro kinase assays (Figures S4G and S4H).

We next asked whether the binding of α-internexin might protect Jacob from dephosphorylation. To address this question, we incubated recombinant MBP-Jacob and pERK1 in the presence or absence of α-internexin fusion proteins of different lengths with mouse brain extracts lacking phosphatase inhibitors. We found that the dephosphorylation of both pJacob and pERK1 was attenuated for periods up to 20 min in the presence of fusion proteins containing C-terminal fragments of α-internexin (Figure 4C). However, when we repeated this assay after disassembly of the protein complex with gel electrophoresis and subsequently incubated the membranes with GST fusion constructs of α-internexin and mouse brain extracts, immunoblotting with anti-pS180-Jacob and anti-pERK1/2 revealed that α-internexin only prevents the dephosphorylation of pJacob, but not of pERK1 (Figure 4D). Taken together, these data point to a scenario in which synaptic NMDARs activate ERK, which then binds and phosphorylates Jacob. This, in turn, enhances the binding of Jacob to a C-terminal fragment of α-internexin, which then prevents dephosphorylation of Jacob and pERK bound to Jacob. The trimeric complex appears to be quite stable and thus well suited for long-distance transport. Indeed, we observed an accumulation of nuclear α-internexin immunofluorescence following enhanced activity of synaptic NMDARs (Figure S5B). Finally, experiments where we knocked down α-internexin with shRNA showed that α-internexin probably stabilizes a transport complex for synapse-to-nucleus

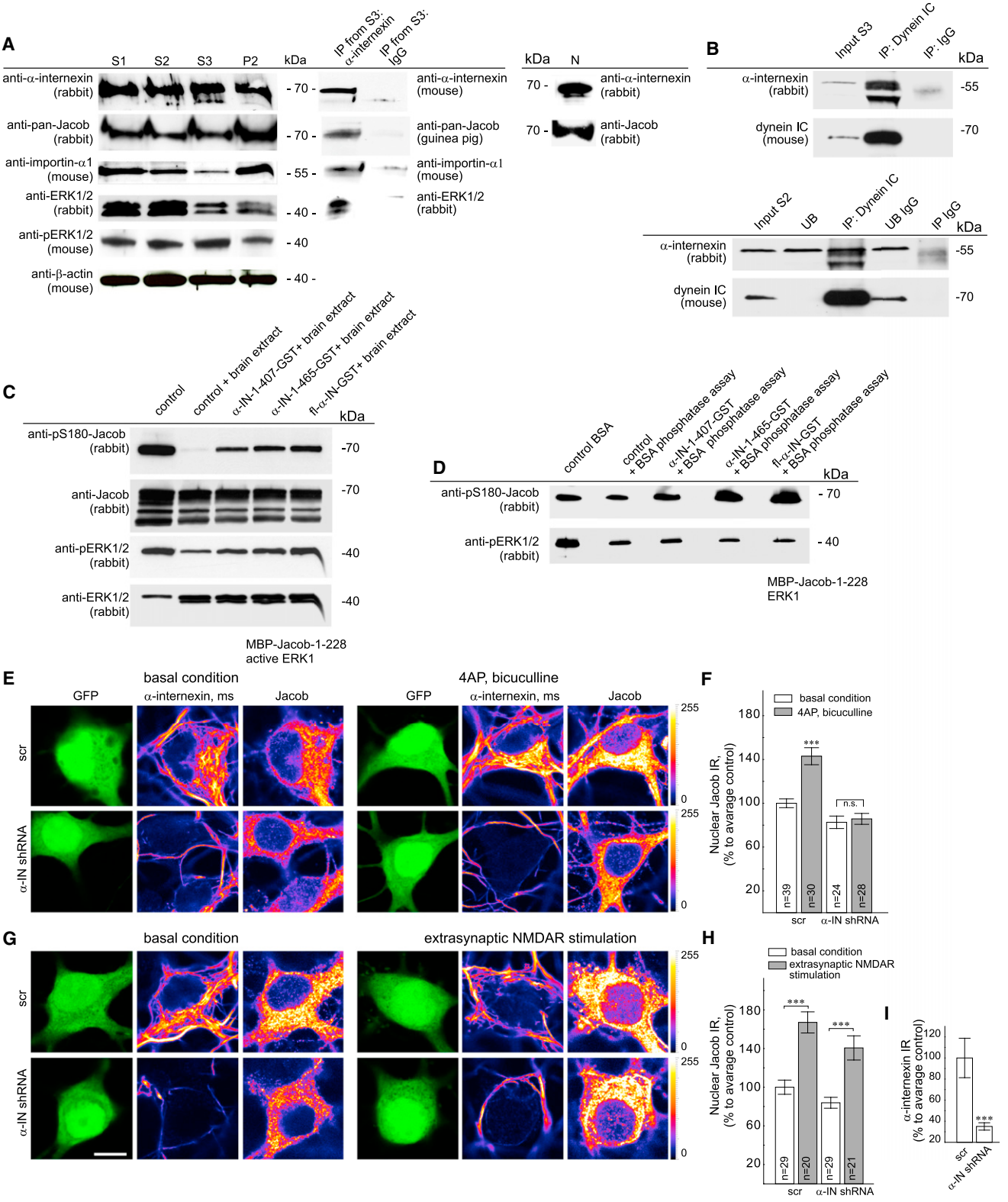

Figure 4. Binding of α-Internexin Protects Jacob against Phosphatase Activity and Is Involved in Nuclear Transit of Jacob upon Enhanced Synaptic Activity

(A) Immunoblotting of Jacob, importin-α1, α-internexin, and ERK in subcellular fractions from adult rat brain. 7 μg of protein was loaded in each lane. S1, pre-cleaned homogenate after centrifugation at 1,000 x *g*; S2, supernatant after removal of mitochondria and heavy membranes by centrifugation at 12,000 x *g*, S3,

(legend continued on next page)

signaling (Figures 4E–4H). In neurons with significantly lower α-internexin levels, the nuclear import of Jacob was significantly reduced after stimulation of synaptic NMDARs (Figures 4G and 4H), but not extrasynaptic NMDARs (Figures 4H and 4I).

pS180-Jacob Accumulates in the Nucleus following the Induction of LTP

We have previously reported that Jacob translocates to the nucleus following the induction of NMDAR-dependent LTP, but not LTD (Behnisch et al., 2011). We found that the induction of chemical LTP was also accompanied by an increase in nuclear pS180-Jacob immunofluorescence, whereas the induction of chemical LTD had the opposite effect (Figures 5A and 5B). To substantiate this finding, we induced and measured the induction of Schaffer collateral LTP in acute brain slices and subsequently isolated neuronal nuclei from CA1 neurons. We first showed that the most prominent pS180 Jacob band in hippocampal CA1 homogenates is not present on immunoblots if the samples are processed in the absence of phosphatase inhibitors (Figure 5C), showing that the antibody does not detect nonphosphorylated endogenous Jacob. We then applied high-frequency stimulation and monitored the induction of LTP for each slice that was subsequently processed for immunoblotting (Figure 5D). Quantitative immunoblotting revealed that, 2 and 30 min following the induction of LTP, pS180 Jacob levels remained unaltered in total CA1 protein homogenates (Figures 5E and 5F), which is not surprising because only a subset of cells will be tetanized. Also, no change in pS180 Jacob levels was observed in nuclear-enriched fractions 2 min after tetanization (Figures 5E and 5F), a time point at which Jacob levels just start to increase in the nucleus following LTP induction (Behnisch et al., 2011). However, we found a 2-fold increase in pS180-Jacob immunoreactivity 30 min after tetanization (Figures 5E and 5F), a time point at which Jacob levels peak in the nucleus (Behnisch et al., 2011). Immunofluorescence stainings confirmed the LTP-induced increase of pS180-Jacob immunoreactivity in nuclei of CA1 neurons (Figure 5G). Thus, Jacob that translocates to the nucleus in a cellular model of learning and memory is phosphorylated at Ser180.

Phosphomimetic and Phosphodeficient Jacob Have Opposite Effects on CREB "Shut-Off," Gene Expression, Cell Survival, and Synaptic Activity

Finally, we asked whether ERK phosphorylation prior to the nuclear entry of Jacob has functional consequences in terms of gene expression, cellular integrity, and synaptic activity. We first investigated whether Ser180 phosphorylation affects the phosphorylation of CREB. N-terminal myristoylation of Jacob is essential for its extranuclear localization (Dieterich et al., 2008). An N-terminal fragment has to be cleaved by calpain before nuclear transit can occur (Kindler et al., 2009). We generated a myristoylation-deficient phosphomimetic mutant, ΔMyr-S180D-Jacob-GFP, that accumulates in the nucleus by default (Figure 6A). Overexpression of ΔMyr-S180D-Jacob-GFP in primary neurons led to a significantly increased pCREB immunofluorescence in the nucleus (Figures 6A, top, and 6B), whereas transfection with the corresponding phosphodeficient mutant ΔMyr-S180A-Jacob-GFP had the opposite effect (Figures 6A and 6B). Interestingly, the increase in pCREB immunofluorescence after nuclear overexpression of phosphomimetic Jacob was also seen in cultures that were silenced by application of TTX, NBQX, and APV (Figures S6A and S6B). Nuclear overexpression of ΔMyr-Jacob leads to CREB shut-off, a drastic simplification of synapto-dendritic complexity, and subsequent cellular degeneration (Dieterich et al., 2008) despite the fact that it can be phosphorylated by ERK. We therefore addressed the question of whether enhanced synaptic activity and the resulting nuclear import of active ERK and subsequent phosphorylation of nuclear ΔMyr-Jacob-GFP (Figures S2E and S2F) might prevent the cellular degeneration seen with this construct. In cultures that were kept in the presence of bicuculline and 4-AP following transfection, enhanced ERK activity was indeed accompanied by increased nuclear pCREB immunostaining in neurons overexpressing ΔMyr-Jacob-GFP (Figures 6A, bottom, and 6B). By contrast, neurons that were transfected with the phosphodeficient mutant ΔMyr-S180A-Jacob showed a CREB shut-off irrespective of the culture conditions (Figures 6A and 6B). As in our previous study (Dieterich et al., 2008), we found a reduced synapto-dendritic complexity under resting conditions in hippocampal neurons expressing either ΔMyr-Jacob-GFP or the phosphodeficient mutant ΔMyr-S180A-Jacob-GFP, but not the phosphomimetic mutant ΔMyr-S180D-Jacob-GFP (Figures 6C–6E). Enhancing synaptic activity with bicuculline and 4-AP led to an almost normal appearance of the ΔMyr-Jacob-GFP transfected neurons (Figure 6E). Moreover, the number of synaptic contacts was unchanged as compared to controls (Figures 6F–6H). Importantly, enhanced synaptic activity could only attenuate the ΔMyr-Jacob-GFP phenotype, but not the phosphodeficient mutant phenotype, strongly supporting the decisive role of

cytosolic nonvesicular fraction obtained after ultracentrifugation of S2 at 100,000 x *g*, P2, crude membranes; and N, purified nuclei. The S3 fraction was subsequently used for coimmunoprecipitation of α-internexin with a pan-Jacob guinea pig antibody.

(B) Dynein intermediate chain coimmunoprecipitates with α-internexin from rat brain S3 and S2 fractions. UB, unbound.

(C) Bacterially expressed recombinant MBP-Jacob-1-228 and active ERK1 were incubated with rat brain extracts containing active phosphatases for 20 min at 30°C. The presence of α-internexin fusion proteins attenuates dephosphorylation of both pJacob and pERK.

(D) α-internexin prevents dephosphorylation of pJacob, but not of pERK1, when ERK is not associated with pJacob. The phosphatase assay was performed on nitrocellulose membranes as described in Extended Experimental Procedures.

(E–H) Small hairpin RNA (shRNA) knockdown of α-internexin significantly reduces nuclear import of Jacob following 4-AP/bicuculline stimulation, but not after stimulation of extrasynaptic NMDARs. (E) and (G) Confocal images of DIV17-18 hippocampal primary neurons transfected with α-internexin shRNA knockdown and corresponding scrambled control constructs (scr). Staining with an anti-α-internexin antibody shows the efficiency of knockdown (lower panels in E and G). α-internexin and pan-Jacob (rabbit) stainings are represented as gradient lookup tables, and quantification is summarized in (F), (H), and (I). Scale bars, 10 μm. Data are represented as mean ±SEM. ***$p < 0.001$ as determined by Bonferroni corrected t tests.

See also Figures S4 and S5.

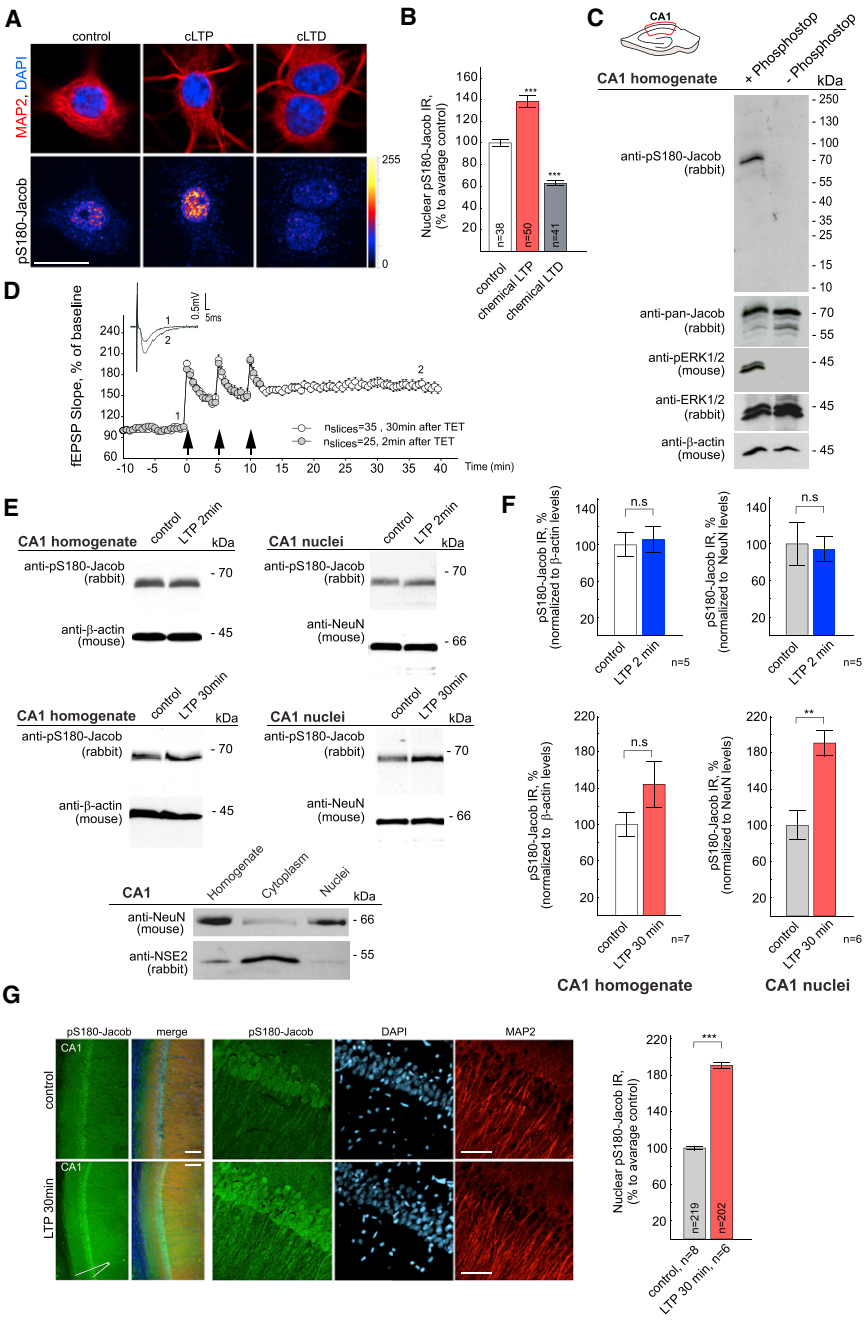

Figure 5. NMDA-Receptor-Dependent LTP Increases Nuclear pS180-Jacob IR

(A) Chemically induced LTP, but not LTD, increases nuclear pS180-Jacob IR in DIV17-18 hippocampal primary neurons. Scale bar, 20 μm.

(B) Intensity-based quantification of nuclear pS180-Jacob IR. Data are represented as mean ±SEM. ***$p < 0.001$ as determined by Bonferroni corrected t tests.

(C) The CA1 region from adult rat hippocampal slices was dissected and homogenized in hypotonic lysis buffer with or without phosphostop (phosphatase inhibitor). The pS180-Jacob and pERK1/2 band were only detected in samples treated with phosphatase inhibitors.

(D–F) Late LTP induced in Schaffer collateral-CA1 synapses results in a significant increase in nuclear pS180-Jacob levels 30 min after tetanization. (D) Averaged field excitatory postsynaptic potentials (fEPSP) slope values over time normalized to 10 min baseline. Insert shows representative traces of evoked fEPSP transients before and 30 min after tetanization. Arrows indicate high-frequency stimulation trains. Slices were shock frozen 2 min or 30 min after induction of LTP.

(E) pS180-Jacob levels in CA1 homogenates and in nuclear-enriched fraction. Five slices were pooled for one preparation, and a total of 25–35 slices was used for each experimental condition. Equal amounts of protein were loaded in each lane. Equal loading was controlled with β-actin (homogenates) and NeuN (nuclei) antibodies. The purity of the preparation was checked with an antibody directed against the cytoplasmic marker protein neuron-specific enolase 2 (NSE2).

(F) Quantification of pS180-Jacob IR normalized to β-actin and NeuN levels, respectively. Data are represented as mean ±SEM. **$p < 0.01$ as determined by Student's t tests.

(G) Late-LTP induced in Schaffer collateral-CA1 synapses results in increased pS180-Jacob staining intensity in nuclei of CA1 pyramidal neurons 30 min after tetanization. Stimulation (position indicated) and recording pipettes were placed in the CA1 stratum radiatum. Depicted are representative sections stained with antibodies directed against pS180-Jacob (green), MAP2 (red), and DAPI (blue) for nuclear detection. Scale bars, 100 μm in the overview and 60 μm in the magnification. Number of slices are indicated below the bar graph. Number of analyzed cells are indicated in each column. Data are represented as mean ±SEM. ***$p < 0.001$ as determined by Bonferroni corrected t tests.

Ser180 phosphorylation for the nuclear function of Jacob (Figures 6C, 6E, 6G, and 6H).

Similar results were obtained in a reporter gene assay in which we cotransfected primary hippocampal neurons with a green fluorescent protein (GFP) construct fused to the BDNF promoter and ΔMyr-S180A- or ΔMyr-S180D-Jacob mutants. The BDNF promoter contains a CRE site, and BDNF expression is a classical readout of CREB transcriptional activity (Figure 7A). Enhancing synaptic activity with bicuculline resulted in increased GFP expression (Figures 7C and 7D). Nuclear overexpression of phosphomimetic Jacob significantly enhanced GFP expression irrespective of synaptic activity, whereas transfection of the phosphodeficient construct had the opposite effect (Figures 7B and 7D).

CREB shut-off has been linked to NMDA-induced cell death and neuronal degeneration. In previous work, we found that a nuclear knockdown of Jacob attenuates NMDA-induced cell death (Dieterich et al., 2008). We therefore asked whether the presence of phosphomimetic Jacob in the nucleus might be neuroprotective. It turned out that phosphomimetic Jacob not

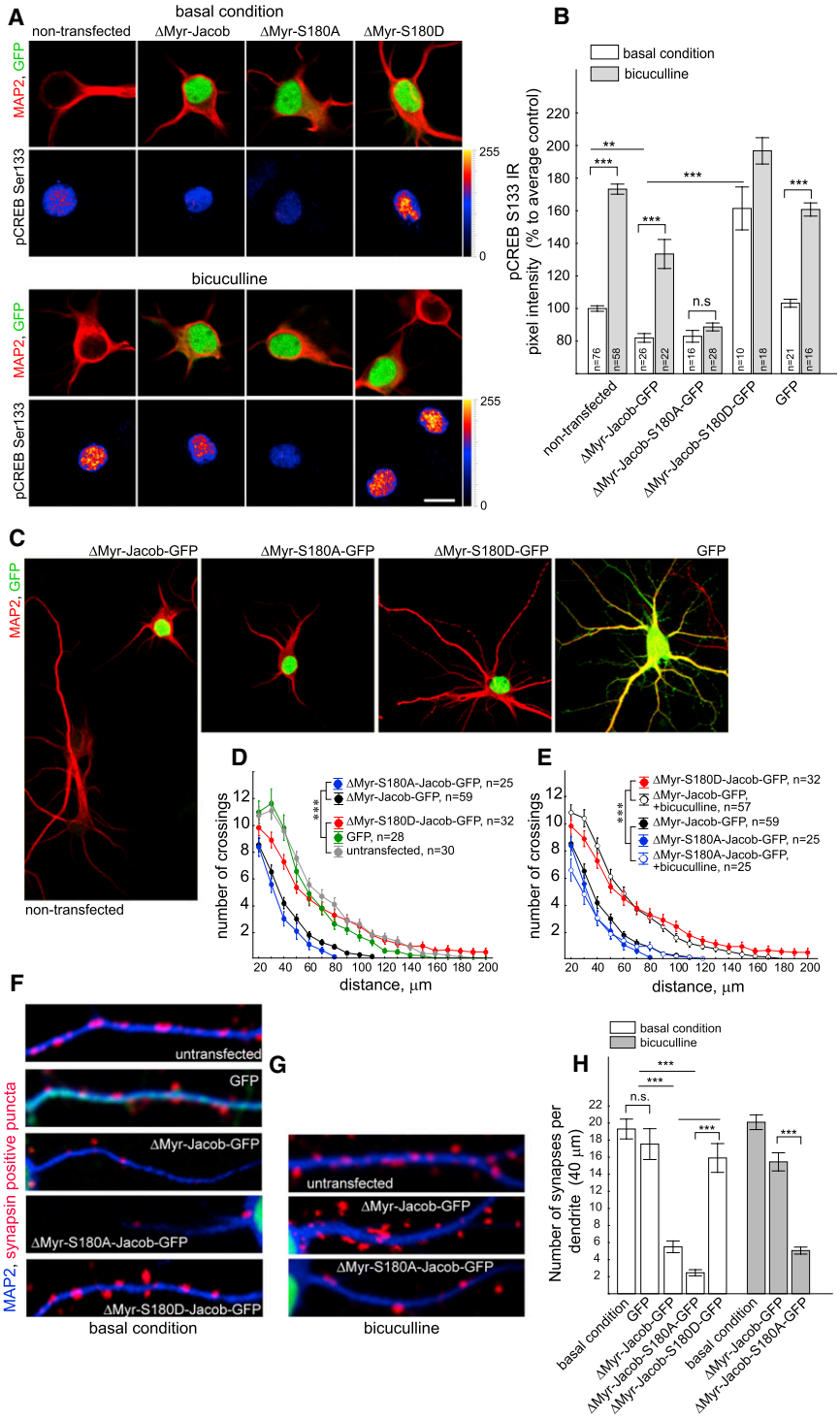

Figure 6. Phosphomimetic (S180D) and Phosphodeficient (S180A) Jacob Regulate CREB Phosphorylation and Synapto-Dendritic Complexity in an Opposing Manner

(A and B) Enhanced synaptic activity induced by 50 μM bicculline (12 hr) abolished CREB shut-off in neurons overexpressing nuclear ΔMyr-Jacob-GFP, but not ΔMyr-Jacob-S180A-GFP. Nuclear overexpression of phosphomimetic Jacob (ΔMyr-Jacob-S180D-GFP) results in increased pCREB IR already under basal conditions. Depicted are confocal images from hippocampal neurons transfected with ΔMyr-Jacob-GFP, ΔMyr-Jacob-S180A-GFP, or ΔMyr-S180D-Jacob-GFP and costained with antibodies against MAP2 (red) and pCREB (gradient lookup table). The PMT gain within each individual experiment was set to a value where the pCREB level after enhanced synaptic activity of NMDAR gave the highest signal without reaching saturation. Scale bar, 20 μm. The diagram (B) represents pixel intensity quantification of pCREB signals normalized to untransfected control. Data are represented as mean ±SEM. $^{**}p < 0.01$ and $^{***}p < 0.001$.

(C–F and H) Neurons overexpressing in the nucleus phosphodeficient Jacob (ΔMyr-Jacob-S180A-GFP) or Jacob that is wild-type with respect to serine 180 (ΔMyr-Jacob-GFP), but not phosphomimetic Jacob (ΔMyr-Jacob-S180D-GFP), exhibit a reduced synapto-dendritic complexity under resting conditions.

(D and E) Overexpression of ΔMyr-Jacob-GFP (black circles) and ΔMyr-Jacob-S180A-GFP (blue circles), but not ΔMyr-S180D-Jacob-GFP (red circles), results in reduced dendritic complexity. The phenotype of ΔMyr-Jacob-GFP, but not ΔMyr-Jacob-S180A-GFP, overexpression can be significantly attenuated by bath application of 50 μM bicuculline (black open circles and blue open circles, respectively) following transfection. The complexity of the dendritic tree was analyzed by Sholl analysis based on MAP2 staining.

(F–H) The synaptic phenotype of ΔMyr-Jacob-GFP, but not of ΔMyr-JacobS180A-GFP, overexpression can be reduced by bath application of 50 μM bicuculline following transfection. (C), (F), and (G) depict confocal images of hippocampal neurons overexpressing Jacob mutants or GFP costained with anti-MAP2 and anti-synapsin antibodies (in F and G). Scale bar, 40 μm. (F and G) Dendrites from cells kept under resting conditions or 21 hr in the presence of bicuculline, respectively. MAP2 staining is indicated in blue; red spots represent presynaptic terminals visualized with anti-synapsin antibody staining. Data are represented as mean ±SEM. $^{***}p < 0.001$ as determined by Bonferroni corrected t tests.

See also Figure S6.

only fostered the phosphorylation of CREB but also significantly reduced apoptosis even in cultures treated with 100 μM NMDA for 5 min (Figures 7E and 7F). Of note, the neuroprotection conferred by overexpression of the phosphomimetic Jacob mutant was still significant 12 hr after the insult, despite the nuclear import of endogenous nonphosphorylated Jacob under these conditions.

The decisive role of ERK phosphorylation for the nuclear function of Jacob is further underscored by the finding that viral expression of ΔMyr-S180D-Jacob, but not of ΔMyr-S180A-Jacob,

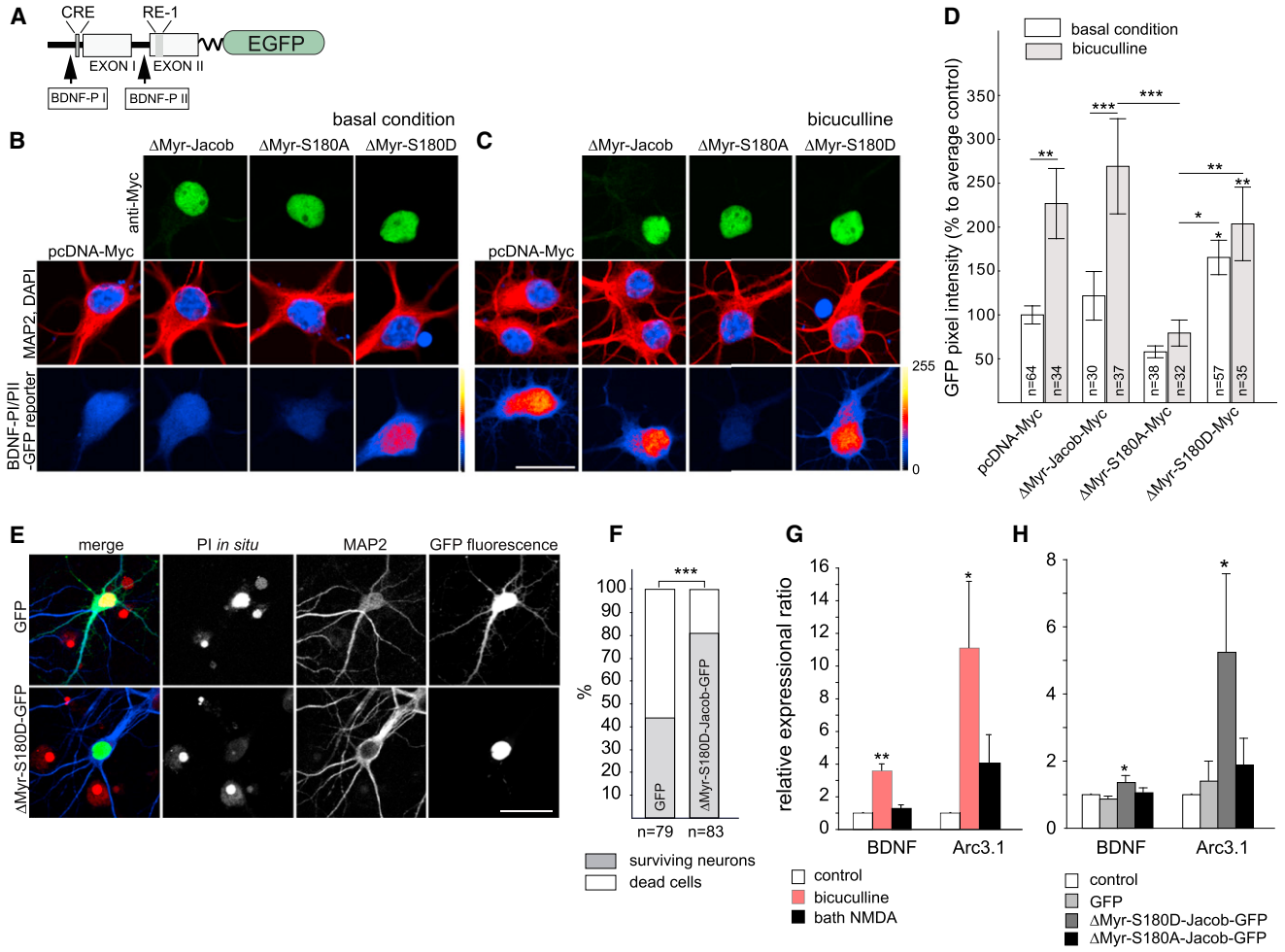

Figure 7. Phosphomimetic S180D and Phosphodeficient S180A Jacob Regulate BDNF Gene Transcription, Cell Death, and Cell Survival in an Opposing Manner

(A–D) Effect of nuclear Jacob overexpression (ΔMyr-Jacob-Myc, phosphomimetic ΔMyr-S180D-Jacob-Myc, or phosphodeficient ΔMyr-S180A-Jacob-Myc mutants) in a BDNF-promoter reporter gene expression system. The lower panel depicts the GFP expression (shown in a gradient lookup table) under basal conditions and in cultures kept in 50 μM bicuculline (B and C). Scale bar, 20 μm.

(D) Intensity-based quantification measured as mean gray value in arbitrary units and normalized to controls. Data are represented as mean ±SEM. *$p < 0.05$, **$p < 0.01$, and ***$p < 0.001$ as determined by Bonferroni corrected t tests.

(E and F) Phosphomimetic Jacob promotes cell survival. Hippocampal neurons were transfected with ΔMyr-Jacob-S180D-GFP or GFP and treated for 5 min with 100 μM bath NMDA at DIV12 followed by 12 hr washout. Neuronal degeneration was monitored by quantification of propidium iodide uptake. Data are represented as mean ±SEM. ***$p < 0.001$ as determined nonparametric Cochran Q-test.

(G) Application of 50 μM bicculline (6 hr) leads to elevated mRNA levels of BDNF and Arg/Arc3.1 as evidenced by quantitative real-time PCR.

(H) Nuclear overexpression of phosphomimetic ΔMyr-Jacob-S180D-GFP in primary neurons kept under basal conditions leads to an increased expression of BDNF and arc/arg3.1. Values in (G) and (H) were normalized to Hprt1. Data are represented as mean ±SEM. *$p < 0.05$ and **$p < 0.01$ in (G) and (H) as determined by Bonferroni corrected t tests.

induces significantly higher transcript levels of the neuronal-plasticity-related genes BDNF and Arc/Arg3.1, resembling an expression pattern seen after enhancing synaptic NMDAR activity in cortical primary cultures (Figures 7G and 7H). Moreover, the gene expression induced by ΔMyr-S180D-Jacob feeds back to synaptic function. Patch-clamp experiments revealed that neurons expressing this construct in the nucleus exhibit a higher mEPSC amplitude, but not mEPSC frequency, as compared to control cells (Figures S6C–S6E). Thus, the gene expression induced by nuclear pS180-Jacob provides a plasticity signal that enhances synaptic efficacy.

DISCUSSION

Here, we provide evidence for a long-distance signaling pathway that encodes the synaptic and extrasynaptic localization of activated NMDARs in the nucleus. Following synaptic NMDAR activation and, in contrast to extrasynaptic NMDAR, Jacob

carries an ERK phosphorylation signature that defines it as a synapto-nuclear protein messenger, designating the synaptic localization of NMDARs that drove its nuclear translocation. Although different signaling mechanisms downstream of both types of NMDARs have been previously described, this study identifies a mechanism that differentiates between these pathways for long-distance signaling. In a physiological context, the pJacob-pERK-α-internexin association provides a new molecular mechanism for a synapto-nuclear protein messenger signalosome involved in long-distance signaling and deciphering of synaptic versus extrasynaptic dendritic signals.

The scenario developed from this and previous studies (Dieterich et al., 2008; Kindler et al., 2009; Behnisch et al., 2011) suggests that, irrespective of receptor localization, NMDAR activation results in the nuclear import of Jacob (Figure S7). Neuronal importin-α can directly associate with NMDARs (Jeffrey et al., 2009), and the translocation process requires the binding of Jacob to importin-α under both conditions, synaptic or extrasynaptic NMDAR activation (Figure S7). In the case of a synaptic origin of the NMDAR signal, pERK will associate with Jacob and phosphorylate Ser180 at synaptic sites, which, in turn, is a prerequisite for Jacob to leave the synapse (Figure S7). It can be tacitly assumed that the activation of ERK at synaptic sites either requires the RasGRF- or the αCamKII-Ras-MEK pathway (Krapivinsky et al., 2003; El Gaamouch et al., 2012). It was suggested that RasGRF1 directly binds to the GluN2B subunit and induces LTD via activation of p38MAP-kinase, whereas RasGRF2 only associates with the GluN2A subunit and is involved in the induction of LTP via activation of ERK (Li et al., 2006). However, the vast majority of synaptic NMDARs are probably triheteromeric (Rauner and Köhr, 2011), and the idea that GluN2A and GluN2B receptors are differentially involved in LTP and LTD induction (Liu et al., 2004) has been challenged (Morishita et al., 2007).

At first glance, it appears unlikely that the phosphorylation signal can be preserved during transport from distal dendrites to the nucleus due to the high phosphatase activity in neurons. However, Perlson et al. (2005) could show that retrograde transport of ERK in axons requires association with importin-β and the molecular motor dynein and that the concomitant binding of vimentin hinders the dephosphorylation of pERK. In analogy to this scenario, we found that C-terminal fragments of α-internexin prevent the dephosphorylation of pJacob and pERK in a trimeric complex. In addition, we observed that this complex is very stable. Knockdown of α-internexin indeed blocked the nuclear import of Jacob after stimulation of synaptic NMDARs, but not extrasynaptic NMDARs. We therefore propose that, analogous to axons, a nonvesicular transport mechanism along microtubuli exists in dendrites, requiring neuronal importins, dynein, and a filament protein that functions as an adaptor to prevent dephosphorylation and the loss of the kinase signal (Figure S7).

Our data suggest that Jacob predominantly exists in a pERK-bound form after synaptic NMDAR activation because the non-phosphorylated kinase binds with considerably lower affinity. However, it should be stressed that Jacob binding only provides a link to active retrograde synapto-nuclear transport for a subfraction of pERK1/2. Facilitated diffusion, rather than active transport, has been postulated to underlie the nuclear accumulation of pERK1/2 in response to enhanced neuronal activity (Wiegert et al., 2007). Also the higher abundance of ERK1/2 precludes a major role of Jacob in the regulation of nuclear ERK1/2 trafficking. In addition, a larger proportion of the synapto-dendritic Jacob pool remains stationary after enhanced synaptic NMDAR activity. The assembly of the proposed pJacob/pERK signalosome at synaptic sites and the details of the transport processes await further clarification. At present, it is unclear if and how this complex is disassembled in the nucleus and why Jacob's trafficking from synapses to the nucleus, but not from extrasynaptic sites, requires ERK phosphorylation.

Nuclear Jacob mediates either cell death or survival (Figure S7). This function seems to be associated with the transcriptional activity of CREB. Jacob is found in complexes that contain DNA and RNA polymerase II (Dieterich et al., 2008), and it can directly associate with CREB (R.K. and M.R.K., unpublished data). This raises the possibility that Jacob might bring signaling components to the CREB complex. It is widely believed that CaMKIV mediates fast CREB phosphorylation at Ser133, whereas ERK1/2 promote CREB phosphorylation in a slower, but more persistent manner (Hardingham et al., 2001; Wu et al., 2001). Our data show that pJacob, pERK, and α-internexin are present in a very stable trimeric complex. It is tempting to speculate that pJacob may possess a scaffolding function for the localization of pERK in nuclear signaling complexes containing CREB after stimulation of synaptic NMDARs. Another yet-to-be-identified mechanism will, in turn, induce CREB shut-off following nuclear import after extrasynaptic NMDAR activation.

The latter function of Jacob suggests that it might be involved in cellular processes associated with extrasynaptic NMDAR activity, including brain ischemia and Huntington's disease (Okamoto et al., 2009; Milnerwood et al., 2010; Tu et al., 2010). However, recent studies also suggest a physiological role of extrasynaptic NMDARs in augmenting synaptic signaling (Harris and Pettit, 2008) as well as in the regulation of homeostatic plasticity (Wang et al., 2011). Glutamate spillover following high-frequency stimulation might stimulate extrasynaptic NMDARs under physiological conditions and elicit nuclear import of Jacob. This is of interest because Jacob can eventually be phosphorylated in various subcellular compartments, and the extrasynaptic versus synaptic pathway might be concomitantly active, leading to a dynamic equilibrium of phosphorylated and nonphosphorylated Jacob complexes translocating into the nucleus (Figure S7). A caveat of the present study is that it lacks proof in vivo. Future work using transgenic mouse models should address this issue.

EXPERIMENTAL PROCEDURES

Expression Constructs, Antibodies, and Primary Cell Culture

A list of all constructs, antibodies, information about the preparation of viruses, immunocytochemical stainings, and live-imaging experiments can be found in Extended Experimental Procedures (Tables S1 and S2).

Subcellular Brain Fractionation and Biochemical Assays

Preparation of PSD-enriched fractions was done as described previously (Dieterich et al., 2008). Pull-down assays were carried out as described previously (Mikhaylova et al., 2009). Further information about the expression and

purification of recombinant proteins and interaction assays can be found in Extended Experimental Procedures.

Biophysical Experiments, Quantitative Real-Time PCR, and Electrophysiology

A detailed description of electrophysiological recordings, messenger RNA (mRNA) experiments, mass spectrometry, and SPR interaction studies is included in Extended Experimental Procedures.

SUPPLEMENTAL INFORMATION

Supplemental Information includes Extended Experimental Procedures, seven figures, and two tables and can be found with this article online at http://dx.doi.org/10.1016/j.cell.2013.02.002.

ACKNOWLEDGMENTS

We want to thank C. Borutzki, M. Marunde, and S. Hochmuth for technical assistance; N. Ziv for helpful discussion; J. Lindquist for proofreading: M. Tsuda, A. Fejtova, D. Ivanova, J. Wiedemann, and U. Thomas for providing constructs; M. Hupe for assistance in α-internexin experiments; A.C. Lehmann for help with cloning; and Y. Chen and P. Yuan Xiang for assistance in electrophysiology. This work was supported by the DFG (SFB 779 TPB8 to M.R.K.; TPZ to T.K. and M.N.; SFB854 TP7 to M.R.K.; TP4 to M.N.; TP8 to E.D.G.; GRK1167 and Kr1879/3-1 to M.R.K.); DIP grant to E.D.G. and M.R.K.; EU FP7 MC-ITN NPlast to M.R.K.; European Regional Development Fund (ERDF 2007–2013); Vorhaben: CBBS to A.K. and C.S.; NSFC 31271197 to T.B.; and the Schram Foundation to M.R.K. M.M. is the recipient of a European Molecular Biology Organization (EMBO) long-term fellowship (EMBO ALTF 884-2011) and is supported by Marie Curie Actions (EMBOCOFUND2010, GA-2010-267146).

Received: May 22, 2012
Revised: December 11, 2012
Accepted: February 1, 2013
Published: February 28, 2013

REFERENCES

Alberini, C.M. (2009). Transcription factors in long-term memory and synaptic plasticity. Physiol. Rev. *89*, 121–145.

Behnisch, T., Yuanxiang, P., Bethge, P., Parvez, S., Chen, Y., Yu, J., Karpova, A., Frey, J.U., Mikhaylova, M., and Kreutz, M.R. (2011). Nuclear translocation of jacob in hippocampal neurons after stimuli inducing long-term potentiation but not long-term depression. PLoS ONE *6*, e17276.

Benson, D.L., Mandell, J.W., Shaw, G., and Banker, G. (1996). Compartmentation of alpha-internexin and neurofilament triplet proteins in cultured hippocampal neurons. J. Neurocytol. *25*, 181–196.

Deisseroth, K., Bito, H., and Tsien, R.W. (1996). Signaling from synapse to nucleus: postsynaptic CREB phosphorylation during multiple forms of hippocampal synaptic plasticity. Neuron *16*, 89–101.

Dieterich, D.C., Karpova, A., Mikhaylova, M., Zdobnova, I., König, I., Landwehr, M., Kreutz, M., Smalla, K.H., Richter, K., Landgraf, P., et al. (2008). Caldendrin-Jacob: a protein liaison that couples NMDA receptor signalling to the nucleus. PLoS Biol. *6*, e34.

El Gaamouch, F., Buisson, A., Moustié, O., Lemieux, M., Labrecque, S., Bontempi, B., De Koninck, P., and Nicole, O. (2012). Interaction between αCaMKII and GluN2B controls ERK-dependent plasticity. J. Neurosci. *32*, 10767–10779.

Flavell, S.W., and Greenberg, M.E. (2008). Signaling mechanisms linking neuronal activity to gene expression and plasticity of the nervous system. Annu. Rev. Neurosci. *31*, 563–590.

Hanz, S., Perlson, E., Willis, D., Zheng, J.Q., Massarwa, R., Huerta, J.J., Koltzenburg, M., Kohler, M., van-Minnen, J., Twiss, J.L., and Fainzilber, M. (2003). Axoplasmic importins enable retrograde injury signaling in lesioned nerve. Neuron *40*, 1095–1104.

Hardingham, G.E., and Bading, H. (2010). Synaptic versus extrasynaptic NMDA receptor signalling: implications for neurodegenerative disorders. Nat. Rev. Neurosci. *11*, 682–696.

Hardingham, G.E., Arnold, F.J., and Bading, H. (2001). A calcium microdomain near NMDA receptors: on switch for ERK-dependent synapse-to-nucleus communication. Nat. Neurosci. *4*, 565–566.

Harris, A.Z., and Pettit, D.L. (2008). Recruiting extrasynaptic NMDA receptors augments synaptic signaling. J. Neurophysiol. *99*, 524–533.

Ivanov, A., Pellegrino, C., Rama, S., Dumalska, I., Salyha, Y., Ben-Ari, Y., and Medina, I. (2006). Opposing role of synaptic and extrasynaptic NMDA receptors in regulation of the extracellular signal-regulated kinases (ERK) activity in cultured rat hippocampal neurons. J. Physiol. *572*, 789–798.

Jeffrey, R.A., Ch'ng, T.H., O'Dell, T.J., and Martin, K.C. (2009). Activity-dependent anchoring of importin alpha at the synapse involves regulated binding to the cytoplasmic tail of the NR1-1a subunit of the NMDA receptor. J. Neurosci. *29*, 15613–15620.

Jordan, B.A., and Kreutz, M.R. (2009). Nucleocytoplasmic protein shuttling: the direct route in synapse-to-nucleus signaling. Trends Neurosci. *32*, 392–401.

Kim, M.J., Dunah, A.W., Wang, Y.T., and Sheng, M. (2005). Differential roles of NR2A- and NR2B-containing NMDA receptors in Ras-ERK signaling and AMPA receptor trafficking. Neuron *46*, 745–760.

Kindler, S., Dieterich, D.C., Schütt, J., Sahin, J., Karpova, A., Mikhaylova, M., Schob, C., Gundelfinger, E.D., Kreienkamp, H.J., and Kreutz, M.R. (2009). Dendritic mRNA targeting of Jacob and N-methyl-d-aspartate-induced nuclear translocation after calpain-mediated proteolysis. J. Biol. Chem. *284*, 25431–25440.

Köhr, G. (2006). NMDA receptor function: subunit composition versus spatial distribution. Cell Tissue Res. *326*, 439–446.

Krapivinsky, G., Krapivinsky, L., Manasian, Y., Ivanov, A., Tyzio, R., Pellegrino, C., Ben-Ari, Y., Clapham, D.E., and Medina, I. (2003). The NMDA receptor is coupled to the ERK pathway by a direct interaction between NR2B and RasGRF1. Neuron *40*, 775–784.

Li, S., Tian, X., Hartley, D.M., and Feig, L.A. (2006). Distinct roles for Ras-guanine nucleotide-releasing factor 1 (Ras-GRF1) and Ras-GRF2 in the induction of long-term potentiation and long-term depression. J. Neurosci. *26*, 1721–1729.

Liu, L., Wong, T.P., Pozza, M.F., Lingenhoehl, K., Wang, Y., Sheng, M., Auberson, Y.P., and Wang, Y.T. (2004). Role of NMDA receptor subtypes in governing the direction of hippocampal synaptic plasticity. Science *304*, 1021–1024.

Mikhaylova, M., Reddy, P.P., Munsch, T., Landgraf, P., Suman, S.K., Smalla, K.H., Gundelfinger, E.D., Sharma, Y., and Kreutz, M.R. (2009). Calneurons provide a calcium threshold for trans-Golgi network to plasma membrane trafficking. Proc. Natl. Acad. Sci. USA *106*, 9093–9098.

Milnerwood, A.J., Gladding, C.M., Pouladi, M.A., Kaufman, A.M., Hines, R.M., Boyd, J.D., Ko, R.W., Vasuta, O.C., Graham, R.K., Hayden, M.R., et al. (2010). Early increase in extrasynaptic NMDA receptor signaling and expression contributes to phenotype onset in Huntington's disease mice. Neuron *65*, 178–190.

Morishita, W., Lu, W., Smith, G.B., Nicoll, R.A., Bear, M.F., and Malenka, R.C. (2007). Activation of NR2B-containing NMDA receptors is not required for NMDA receptor-dependent long-term depression. Neuropharmacology *52*, 71–76.

Okamoto, S., Pouladi, M.A., Talantova, M., Yao, D., Xia, P., Ehrnhoefer, D.E., Zaidi, R., Clemente, A., Kaul, M., Graham, R.K., et al. (2009). Balance between synaptic versus extrasynaptic NMDA receptor activity influences inclusions and neurotoxicity of mutant huntingtin. Nat. Med. *15*, 1407–1413.

Papadia, S., Soriano, F.X., Léveillé, F., Martel, M.A., Dakin, K.A., Hansen, H.H., Kaindl, A., Sifringer, M., Fowler, J., Stefovska, V., et al. (2008). Synaptic NMDA receptor activity boosts intrinsic antioxidant defenses. Nat. Neurosci. *11*, 476–487.

Perlson, E., Hanz, S., Ben-Yaakov, K., Segal-Ruder, Y., Seger, R., and Fainzilber, M. (2005). Vimentin-dependent spatial translocation of an activated MAP kinase in injured nerve. Neuron *45*, 715–726.

Perlson, E., Michaelevski, I., Kowalsman, N., Ben-Yaakov, K., Shaked, M., Seger, R., Eisenstein, M., and Fainzilber, M. (2006). Vimentin binding to phosphorylated Erk sterically hinders enzymatic dephosphorylation of the kinase. J. Mol. Biol. *364*, 938–944.

Rauner, C., and Köhr, G. (2011). Triheteromeric NR1/NR2A/NR2B receptors constitute the major N-methyl-D-aspartate receptor population in adult hippocampal synapses. J. Biol. Chem. *286*, 7558–7566.

Rönicke, R., Mikhaylova, M., Rönicke, S., Meinhardt, J., Schröder, U.H., Fändrich, M., Reiser, G., Kreutz, M.R., and Reymann, K.G. (2011). Early neuronal dysfunction by amyloid β oligomers depends on activation of NR2B-containing NMDA receptors. Neurobiol. Aging *32*, 2219–2228.

Thomas, G.M., and Huganir, R.L. (2004). MAPK cascade signalling and synaptic plasticity. Nat. Rev. Neurosci. *5*, 173–183.

Thompson, K.R., Otis, K.O., Chen, D.Y., Zhao, Y., O'Dell, T.J., and Martin, K.C. (2004). Synapse to nucleus signaling during long-term synaptic plasticity; a role for the classical active nuclear import pathway. Neuron *44*, 997–1009.

Tu, W., Xu, X., Peng, L., Zhong, X., Zhang, W., Soundarapandian, M.M., Balel, C., Wang, M., Jia, N., Zhang, W., et al. (2010). DAPK1 interaction with NMDA receptor NR2B subunits mediates brain damage in stroke. Cell *140*, 222–234.

Wang, C.C., Held, R.G., Chang, S.C., Yang, L., Delpire, E., Ghosh, A., and Hall, B.J. (2011). A critical role for GluN2B-containing NMDA receptors in cortical development and function. Neuron *72*, 789–805.

Wiegert, J.S., Bengtson, C.P., and Bading, H. (2007). Diffusion and not active transport underlies and limits ERK1/2 synapse-to-nucleus signaling in hippocampal neurons. J. Biol. Chem. *282*, 29621–29633.

Wu, G.Y., Deisseroth, K., and Tsien, R.W. (2001). Activity-dependent CREB phosphorylation: convergence of a fast, sensitive calmodulin kinase pathway and a slow, less sensitive mitogen-activated protein kinase pathway. Proc. Natl. Acad. Sci. USA *98*, 2808–2813.

Yuan, A., Rao, M.V., Sasaki, T., Chen, Y., Kumar, A., Veeranna, Liem, R.K., Eyer, J., Peterson, A.C., Julien, J.P., and Nixon, R.A. (2006). Alpha-internexin is structurally and functionally associated with the neurofilament triplet proteins in the mature CNS. J. Neurosci. *26*, 10006–10019.

Zhang, S.J., Steijaert, M.N., Lau, D., Schütz, G., Delucinge-Vivier, C., Descombes, P., and Bading, H. (2007). Decoding NMDA receptor signaling: identification of genomic programs specifying neuronal survival and death. Neuron *53*, 549–562.

Zhang, S.J., Buchthal, B., Lau, D., Hayer, S., Dick, O., Schwaninger, M., Veltkamp, R., Zou, M., Weiss, U., and Bading, H. (2011). A signaling cascade of nuclear calcium-CREB-ATF3 activated by synaptic NMDA receptors defines a gene repression module that protects against extrasynaptic NMDA receptor-induced neuronal cell death and ischemic brain damage. J. Neurosci. *31*, 4978–4990.

EXTENDED EXPERIMENTAL PROCEDURES

Expression Constructs and Generation of Recombinant Semliki Forest and Lentiviral Particles

Both, full length (wild-type, WT, aa 1-532 Gene ID: 117536) Jacob (WT-Jacob-GFP) and a Jacob construct where glycine at the second position was substituted by alanine (ΔMyr-Jacob-GFP, G2A, Dieterich et al., 2008) for nuclear localization were used as templates for the production of eukaryotic and bacterial expression constructs listed in Table S1. Phosphodeficient (substitution of serine at position 180 to alanine, S180A) and phospho-mimetic (substitution of serine to aspartate, S180D) constructs were created by site directed mutagenesis using the QuikChange Kit (Agilent Technologies, Santa Clara, CA) according to the supplier's manual and verified by sequencing analysis.

WT-Jacob-GFP, ΔMyr-Jacob-GFP, ΔMyr-Jacob-S180A-GFP and ΔMyr-Jacob-S180D-GFP were subcloned into the pSFV1 vector (Invitrogen, Life Technologies, Darmstadt, Germany). The protocol for production of the Semliki Forest viral (SFV) particles was described previously (Karpova et al., 2006; Dieterich et al., 2008). Briefly, linearized recombinant pSFV1-Jacob-GFP and pSFV-Helper2 plasmids were transcribed in vitro using the mMESSAGE mMACHINE High Yield Capped RNA Transcription Kit (Ambion, Life Technologies, Darmstadt, Germany). RNA quality was checked on an agarose gel. Both RNAs were co-transfected into packaging CHO-K1 cells using Lipofectamine 2000 (Invitrogen) according to the manufacturer's protocol (Invitrogen, Karlsruhe, Germany). F12 Nutrient Media (GIBCO, Invitrogen) were collected 24, 48 and 72 hr after transfection and particles were concentrated by ultracentrifugation in a 10% sucrose gradient. Aliquots of the inactive virus were stored at −80°C in 30% sucrose storage solution. Shortly before infection, SFV particles were activated with α-chymotrypsin (10 mg/ml, Sigma-Aldrich, Taufkirchen, Germany) for 45 min at room temperature followed by chymotrypsin inactivation with aprotinin (0.5 mg/ml Sigma). The virus was used for infection of primary neuronal cultures within the next three days.

For Lentiviral particle production HEK293T cells plated in 75 cm^2 flasks were co-transfected with psiHIV-H1 (HIV based) plasmids containing shRNA against α-internexin (RSH049887-HIVH1) or scrambled shRNA (CSHCTR001-HIVH1) together with the Lenti-Pac HIV expression packaging mix (HPK-LvTR-20) provided by the supplier (all GeneCopoeia, Rockville, Maryland) according to manufacturer's instructions. Two days post-transfection DME Medium (GIBCO) containing the viral particles was collected and stored at −80°C.

Compounds and Pharmacological Treatments

Anisomycin (7.5 μM), 4-Aminopyridine (4-AP, 2.5 mM) and MK801 (10 μM) were obtained from Sigma (Munich, Germany). NMDA (5 μM, 20 μM, 50 μM, 100 μM), bicuculline methiodide (50 μM), CNQX (10 μM) and NBQX (10 μM) were purchased from Tocris bioscience (Bristol, UK), D-AP5 (20 μM), U0126 (10 μM) from Cell Signaling Technology (Darmstadt, Germany), roscovitine (10 μM) and tetrodotoxin (TTX, 1 μM), from Alomone labs (Munich, Germany).

To examine the role of ERK1/2 and CDK5 in the nuclear transport of Jacob the MEK inhibitor U0126 and the CDK5 inhibitor roscovitine were added to the culture medium 1h prior the stimulation. To silence synaptic activity neurons were incubated with TTX, D-AP5 and CNQX or NBQX. The protocol used for synaptic and extrasynaptic NMDAR stimulation of hippocampal primary neurons was described previously (Dieterich et al., 2008; Behnisch et al., 2011). Briefly, synaptic NMDARs were stimulated by modulating network activity by blocking of both GABAergic inhibition with bicuculline and repolarisation by 4-AP. For extrasynaptic NMDAR stimulation cultures were first stimulated as described above, in the presence of the non-competitive NMDAR antagonist MK801 to inactivate synaptic NMDARs. The culture medium was replaced 25 min after the treatment in order to remove unbound MK801. Since synaptic NMDARs have been blocked by MK801, subsequent NMDA treatment activated only extrasynaptic receptors. To stimulate the extrasynaptic NMDAR population 100 μM NMDA was applied to the bath medium for 3 min followed by a 30 min washout. The experiments were repeated at least three times. Chemical LTP and LTD protocols were described previously (Lu et al., 2001; Behnisch et al., 2011).

Neuronal Cultures and Transfection

Hippocampal and cortical rat (from E18-E19 and P0-P3) and mouse (from P1) primary cultures were prepared as described previously (Bekkers and Stevens, 1989; Dieterich et al., 2008; Behnisch et al., 2011) and conducted under established standards of the German federal state of Saxony-Anhalt, Germany in accordance with the European Communities Council Directive 2010/63/EU. Primary neurons were kept in Neurobasal medium (NB/GIBCO/Life Technologies) supplemented with B27 (GIBCO/Life Technologies), L-Glutamine (GIBCO/Life Technologies) and penicillin/streptomycin (*PAA* Laboratories, Pasching, Austria). On day 5-6 after plating hippocampal neurons were treated with 5 μM Cytosine D-Arabino-Furanoside (Sigma-Aldrich) in order to prevent proliferation of non-neuronal cells.

Neurons were transfected with cDNA plasmids using Lipofectamine 2000 transfection reagent (Invitrogen) according to the protocol described by Kapitein et al. (2010). For life imaging experiments neurons were transfected at DIV14/15 and kept for additional 18-24 hr before time-lapse image acquisition. For quantitative immunodetection of pCREB(Ser133) and analysis of synaptodendritic morphology ΔMyr-Jacob-GFP, ΔMyr-Jacob-S180A-GFP, ΔMyr-Jacob-S180D-GFP constructs were transfected at DIV9/10 and neurons were fixed 24 hr after.

For the BDNF-promoter reporter assay DIV10 primary hippocampal neurons were co-transfected with equal amounts of BDNF-PI/PII-GFP reporter construct (Hara et al., 2009) and one of the Jacob constructs (ΔMyr-Jacob-Myc, ΔMyr-Jacob-S180A-Myc,

ΔMyr-Jacob-S180D-Myc) or empty pcDNA3.1 vector. 18 hr post-transfection neurons were stimulated for 6 hr with 50 μM bicuculline, subsequently fixed and processed for immunostainings as described below. Expression of GFP under the control of the endogenous BDNF promoter was quantified.

For cell death assay ΔMyr-Jacob-S180D-GFP and GFP plasmids were expressed at DIV5 and neurons were fixed at DIV12 twelve hours after NMDA stimulation (100 μM for 3 min). Older (DIV16-18, DIV19/23 and DIV28/30) high-density primary hippocampal and cortical cultures were infected with Jacob recombinant SFV particles. In all experiments using Lenti virus based protein knock down hippocampal primary neurons were either infected with Lenti shRNA viral particles by adding 100 μl of Lenti-virus containing media to the culture at the day of plating with media exchange at the next day or transfected with psiHIV-H1 plasmids containing shRNA at DIV4-5 using Lipofectamine 2000 (Invitrogen).

Immunocytochemistry and Antibodies

Cells were fixed in 4% paraformaldehyde in PBS for 10 min, washed three times in PBS, permeabilized with 0.2% Triton X-100 in PBS for 10 min, washed three times and blocked in blocking buffer containing 2% BSA for one hour. Primary antibodies diluted in the blocking buffer were applied overnight at 4°C. Cells were washed and incubated with an appropriate secondary antibody diluted in blocking solution for 1.5 hr. Coverslips were subsequently washed in PBS, rinsed in water and mounted either in Vectashield with DAPI (Vector Laboratories Inc. /Enzo Life Sciences, Lörrach, Germany) or in Mowiol 4-88 (Calbiochem/ Merck Chemicals Ltd., Nottingham, United Kingdom).

The rabbit anti-Jacob antibody (Jb150; peptide sequences used for immunization were *RERSFSRSWSDPTPM* – aa 285-299 and *KADTSHDSRDSSDLQ* - aa 300-314) and the guinea pig anti-Jacob antibody (Jac2gp2) generated against GST fusion proteins (GST-Jacob-253–404) were described previously (Dieterich et al., 2008). A novel rabbit Jacob peptide antibody (Jacob-1384) was raised against the peptide sequence *MKADTSHDSRDSSDLQ* (aa 299-314) and a polyclonal serum was obtained after immunization of rabbits with an MBP-fusion protein (MBP-Jacob-1-228). All antisera were affinity purified using corresponding fusion proteins (GST/MBP-Jacob-1-228, GST/MBP-Jacob-262-531). A synthetic phosphorylated peptide LVPGpSPRAFG corresponding to amino acids 178-187 of the rat Jacob sequence was used to produce the phospho-specific pS180-Jacob antibody (BioGenes, Berlin, Germany). The affinity-purified phosphospecific (pS180-Jacob) antiserum was tested for specificity by immunoblots (dilution 1:100), on homogenates of ΔMyr-Jacob-GFP expressing HEK293 cells as well as by ICC (dilution 1:30) on hippocampal primary neurons.

To detect the activated form of ERK and to control its inhibition after treatment with the MEK1/2 inhibitor U0126, commercial monoclonal antibody (M9692, Sigma-Aldrich) raised against a dually phosphorylated synthetic peptide HTGFLpTEpYVAT corresponding to the activated form of ERK was used. The rabbit anti-pCREB (Ser133) immunoaffinity purified IgG was obtained from Upstate (Temecula, USA). The following synapto-dendritic markers were used: rabbit *polyclonal antisera* against *synapsin* (Synaptic Systems, Göttingen, Germany), polyclonal anti-Homer produced in rat (Acris Antibodies, Herford, Germany), purified Oyster-550 fluorescence-labeled mouse monoclonal IgG against synaptotagmin-1 luminal domain (Synaptic Systems), affinity purified mouse anti-Bassoon (Synaptic Systems) and purified mouse antibody to MAP2 (Sigma-Aldrich). The α-internexin antibodies were obtained from Abcam (rabbit polyclonal ab7259 and ab30326) raised against recombinant full length protein as well as from Covance (1D2, mouse. Princeton, New Jersey, USA) raised against C-terminal non-helical extension of the protein. In addition to antibodies described above, the commercial antibodies used in the study are listed below in the Table S2.

Confocal Laser Scanning Microscopy and Image Analysis

The SP2 and SP5 CLSM systems (Leica-Microsystems, Mannheim, Germany) equipped with Diode (405nm), Argon (458, 476, 488, 496, 514 nm laser lines), Diode Pumped Solid State (DPSS, 561nm) and HeNe (633nm) lasers and acousto-optic tunable filters (AOTF) for selection and intensity adaptation of laser lines using LAS AF (Leica Application Suite Advanced Fluorescence) imaging software were used for quantitative ICC and time-lapse imaging. Quick Change Chamber 18 mm Low Profile RC-41LP (Warner Instruments) was used for mounting coverslips with living cells in NB (GIBCO) on the microscope stage. Images were taken with Plan Apo 63x oil NA 1.4 or Plan Apo 100x oil NA 1.4 objective lenses. All images were acquired sequentially to avoid crosstalk between channels. Along the z-axis usually 5 to 9 optical sections with a focus depth of 0.3 to 0.6 μm were scanned in a 512x512 pixel format at 8 bit image depth with two times frame average at 200 Hz laser frequency. Images from stimulated and non-stimulated cultures were acquired with the same settings for all samples within one experimental group. Subsequently, image analysis was carried out with the ImageJ software (NIH, http://rsb.info.nih.gov/ij/) as described previously (Dieterich et al., 2008; Behnisch et al., 2011). Nuclear immunoreactivity was determined with a DAPI staining as the defining parameter for the region of interest. In addition, the complexity of the dendritic arbors in neurons overexpressing nuclear Jacob was analyzed based on the MAP2 staining, employing Sholl analysis. Particularly, the number of dendrite crossings with a series of concentric circles around the soma of the neuron was quantified by an internal algorithm of the Sholl-analysis plug-in in ImageJ (NIH). Synaptic Jacob levels were quantified using Open View custom analysis software (N. Ziv, Rappaport Institute, Haifa, Israel; Tsuriel et al., 2006). Homer positive puncta were used as ROI and colocalized Jacob immunofluorescence was quantified. Puncta lacking adjacent Bassoon staining were excluded from the analysis. All Jacob intensity values per field of view (~100 Homer/ Bassoon positive puncta) were averaged and normalized to control average.

Subcellular Brain Fractionation

Preparation of PSD enriched fraction was done as described previously (Seidenbecher et al., 1998; Smalla et al., 2003). For isolation of the membrane-free cytosolic fraction, a protocol modified from Hradsky et al. (2011) was used.

Protein Extraction from Transfected HEK293 Cells

Transfected HEK293 cells were scraped in growth media, collected into a 15 ml falcon tube and spun at 1 500 x g at 4°C for 3 min. The cell pellets were washed with 1xTBS and transferred into a 1.5 ml eppendorf tube for lysis. After washing, 400-800 μl of extraction buffer (1xTBS plus 1% Triton X-100 and Roche proteinase inhibitor without EDTA, complete, Roche) was added to each sample and the cells were subjected to freezing in liquid nitrogen and thawing steps twice and incubated afterward at 4°C for 60 min. Finally, the cell lysates were centrifuged at 20 000 x g for 20 min and the supernatant was used in pull down and co-immunoprecipitation experiments.

Pull-Down Assays

GST-Jacob and Recombinant ERK1

Beads with GST fusion constructs of Jacob were preincubated with 2.5% BSA in 1xTBS buffer containing 7 mM Mg^{2+} for 15 min at RT to block unspecific binding. 50 ng of recombinant active or inactive ERK1 were added to the reaction and incubated for 1 hr at RT on slow rotator. Subsequently beads were extensively washed and proteins were eluted with 2x SDS loading dye.

WT-Jacob-Myc and GST-fl-α-Internexin

The extracts from HEK293 cells transfected with WT-Jacob-Myc construct were prepared as described above. Equimolar amounts of the GST-fl-α-internexin fusion protein and GST-coupled sepharose beads were washed three times with ice cold extraction buffer and spun at 300 x g at 4°C for 3 min after each wash. After washing, 500 μl of HEK293 cell extracts were added to the prewashed GST-fl-α-internexin and GST-coupled sepharose beads and each of the reaction mixtures were filled up to 1 ml by the addition of extraction buffer. The reaction mixtures were incubated overnight at 4°C on a tube rotator. Afterward, the samples were spun at 300 x g at 4°C for 3 min, washed with the extraction buffer three times and spun with the same settings after each wash. The bound fraction was re-suspended in 40 μl of 2x SDS sample loading buffer and analyzed by immunoblotting.

GST-fl-α-Internexin and GST-Jacob with Endogenous ERK1/2

Rat brain extract and HEK293 cell lysates were used as a source of endogenous ERK-1/2 and were incubated with equimolar amounts of pre-washed GST-fl-α-internexin, different GST-Jacob fusion proteins or GST-coupled sepharose beads overnight at 4°C on a tube rotator. For pull down experiments with GST-Jacob, beads were blocked with 2.5% BSA for 15 min prior to the experiment. Afterward, the samples were spun at 500 rpm at 4°C for 5 min, washed with the extraction buffer (TBS, 1% Triton X-100, protease inhibitor cocktail /complete, Roche/ and phosphatase inhibitor cocktail /PhosSTOP, Roche) three times and spun at 500 rpm at 4°C for 5 min after each wash. The bound fraction was re-suspended in 40 μl of 2x SDS sample loading buffer and analyzed by immunoblotting.

Immunoprecipitation of the Endogenous Jacob-ERK1/2 Complex

Immunoprecipitation of endogenous Jacob-ERK1/2 complexes were performed from rat brain extracts (1xTBS, 1%Triton X-100, 2 mM Mg^{2+}, protease inhibitor cocktail, pH 7.5) as described previously (Dieterich et al., 2008). Briefly, pre-immuneserum for Jac2gp2 or immuneserum, containing Jac2gp2 antibody were covalently cross-linked to Protein A sepharose beads (GE Healthcare). Beads were blocked with 1.5% BSA for 30 min at 4°C. Rat brain extract was incubated with the antibody bound beads overnight. Then unbound fraction was removed, sepharose was extensively washed in extraction buffer and proteins were eluted with 2x SDS loading dye and subjected to SDS-PAGE.

Immunoprecipitation Experiments from S2 and S3 Brain Fractions

Soluble non-vesicular brain fraction was incubated with the antibody against α-internexin (rabbit α-internexin, Abcam 30326, Germany) or corresponding rabbit IgG control overnight at 4°C. Protein G sepharose beads (GE Healthcare) were washed 3 times with cold homogenization buffer (10 mM HEPES PH 7.4; 150 mM NaCl; 2 mM $MgCl_2$; 1 mM DTT; 2 x protease inhibitor cocktail (Complete, Roche)), blocked with 1.5% BSA for 30 min at 4°C and then incubated overnight with a soluble non-vesicular brain protein fraction and rabbit α-internexin antibody for three hours at 4°C. Afterward, the samples were spun at 300 x g at 4°C for 3 min, washed with the homogenization buffer 3 times and spun with the same settings after each wash. The bound fraction was resuspended in 40 μl of 2x SDS sample loading buffer and analyzed by immunoblotting. Detection of proteins in the complex was performed with mouse α-internexin antibody (Covance), Jac2gp2 antibody, mouse importin-α1 (BD Bioscience) and rabbit Erk (Stressgen).

Expression and Purification of Recombinant Proteins in *E. coli*

MBP Purification

MBP-Jacob-1-228 and MBP-Jacob-262-531 were purified from IPTG-induced BL21 (RIPL) bacteria as described previously (Dieterich et al., 2008).

GST Purification

GST-Jacob and GST-α-internexin constructs were expressed in E. Coli BL21(DE3). 0.1-0.5 mM of IPTG was used to induce the expression of the fusion proteins. C-terminal Jacob constructs were induced for 3-4 hr at 37°C, GST-Jacob-45-280 was induced at 20°C for 4 hr. Subsequently, cells were spun down by centrifugation at 6.000xg and pellets were re-suspended in a cold PBS buffer containing protease inhibitor cocktail. Passing the bacterial suspension via French press and subsequent ultrasonication destroyed cell walls and the proteins were extracted over 1 hr by addition of 1% Triton X-100. The soluble fraction obtained after centrifugation of the cell lysate at 12.000xg for 30 min was loaded on a glutathione sepharose (GE Healthcare) column. Further steps of purification were done as described previously (Mikhaylova et al., 2009). For production of active pERK1, the GST-ERK1 was co-expressed with constitutively active mutant of MEK1 (for construct information see Table S1). Purification of active GST-ERK was done in the presence of 7 mM Mg^{2+} and 100 μM ATP in the lysis buffer. The efficiency of phosphorylation was analyzed by immunoblotting with phospho-ERK1 specific antibody.

6xHis-Tag Purification

6xHis-SUMO-Jacob-Δ1-44 (mouse and rat sequences) were purified from IPTG induced BL21 (RIPL) cells. In order to increase the solubility of the fusion protein, bacteria were induced with 0.1 mM IPTG at 18°C for 6 hr. Purification with the ProBondTM purification system (Invitrogen, Karlsruhe, Germany) was done as published previously (Mikhaylova et al., 2009). Furthermore, to increase the purity of the fusion proteins and to allow exchange of the buffer to, for instance, a buffer suitable for the SPR measurements, gel filtrations on HiLoad SuperdexTM 75 16/60 or SuperdexTM 75 10/300 GL columns (GE Healthcare, Munich, Germany) were performed. Purified proteins were finally concentrated using Amicon 15 Centrifugal filter devices (Millipore, Schwalbach, Germany) with 3 or 10 kDa cut off size.

μ-Calpain Cleavage Assay of α-Internexin In Vitro

For each reaction 1.0 μg purified recombinant GST-α-internexin-1-407, GST-α-internexin-1-465 or GST-fl-α-internexin was used and samples containing GST-fl-α-internexin were incubated with 0.2 units of μ-Calpain (specific activity 0.195 units) along with 2 mM $CaCl_2$ or with 2 mM EGTA and the final reaction volume was adjusted to 20 μl with TBS buffer. Samples without μ-Calpain, $CaCl_2$ and EGTA were used for control reaction. The cleavage reaction was carried out at 30°C for 10 s, 30 s and 1 min and were terminated by addition of 5 μl of 4x SDS sample buffer and samples were analyzed by immunoblotting.

Yeast Two-Hybrid Assay

The Matchmaker GAL4 Two-Hybrid System3 (Takara Bio Europe/Clontech, France) was used for Jacob-α-internexin interaction assay. The fusion vectors (bait vector pGBKT7, prey vector pGADT7,) were introduced to the yeast reporter strain AH109 by the Lithium acetate/ single-stranded carrier DNA/polyethylene glycol (LiAc/SS-Carier DNA/PEG) transformation method (Gietz and Woods, 2002). All constructs were tested for toxicity and self-activation before performing interaction studies. Co-transformed yeasts were assayed for growth on quadruple drop-out medium (SD/–Ade/–His/–Leu/–Trp) and additionally for LacZ reporter activation according to the manufacturer's protocol.

Phosphatase Protection Assays

Phosphatase Assay in Solution

For the first approach, equal volumes of the kinase reaction (about 0.2 μg of MBP-Jacob-1-228 and 0.05 μg of pERK1 per individual reaction) were mixed with equimolar amounts (approximately 0.5 μg) of recombinant purified GST-α-internexin-1-407, GST-α-internexin-1-465, GST-fl-α-internexin or GST control and incubated for 30 min on ice. Freshly prepared mouse brain extracts were used as a source of phosphatases. One adult mouse brain was homogenized in 10 ml of extraction buffer (1xTBS, 1% Triton X-100, EDTA free Protease Inhibitor Cocktail from Roche, pH 7.4), incubated for 40 min at 4°C and centrifuged for 30 min at 12.000 rpm. 10 μl of the supernatant fraction were used for each phosphatise reaction. Control samples were treated only with the extraction buffer. Dephosphorylation was performed for 20 min at 30°C and terminated by addition of denaturing SDS loading dye.

Phosphatase Assay on Nitrocellulose Membranes

As a second approach, the kinase reaction was directly mixed with SDS loading dye, boiled and subjected to SDS-PAGE. After transfer, the membrane was cut in individual strips and blocked with 2%BSA in 1xTBS for 30 min at RT. Sequentially, the membrane strips were pre-incubated with the different GST-α-internexin fusion proteins, diluted in the blocking buffer (approximately 5 μg in 4 ml) for 1 hr at 4°C, washed two times with TBS and incubated with mouse brain extract for 30 min at RT.

Phosphorylation Analysis by Mass Spectrometry

Primary cortical neurons plated at a density of $4x10^6$ cells per 75 cm^2 flask were infected with WT-Jacob-GFP using SFV at DIV18 and kept for 12 hr for phosphorylation by endogenous neuronal activity enhanced by addition of 50 μM bicuculline or were silenced by application of 1 μM of TTX. Nuclear extracts from infected cells were prepared as described before (Dieterich et al., 2008) and Jacob-GFP was purified using the μMACSTM GFP Isolation Kit (Miltenyi Biotec GmbH, Cologne, Germany) according to the manufacturer's protocol. Eluted samples were separated by SDS-PAGE. The bands corresponding to Jacob-GFP were detected by immunoblotting with anti-GFP mouse (Covance, Munich, Germany) and anti-pS180-Jacob rabbit antibodies. Corresponding areas showing pJacob-IR on immunoblots were cut out from the coomassie blue stained SDS-PAGs. Gel pieces underwent in-gel digestion according to

Shevchenko et al. (1996) and were subjected to a nanoLC-ESI-Iontrap mass spectrometer. Samples from in vitro kinase assays were digested and the phospho-peptides were enriched by 5 μm TiO-spheres (GL Sciences Inc., Japan). Resulting peptides were subjected to a nano-reversed phase (C18)-HPLC on-line coupled to an Esquire HCT ETDII-Iontrap mass spectrometer (Bruker Daltonik GmbH, Bremen, Germany). MS/MS precursor selection was tuned for the preferential use of masses corresponding to double (852.36 Da) and triple charged ions (568.57 Da) of the putative *ECPGCAQLVPGPpSPR* Jacob peptide.

Surface Plasmon Resonance

Surface plasmon resonance (SPR) studies for Jacob-ERK1 binding were performed on a Biacore 2000 instrument (GE Healthcare, Munich, Germany) at 25°C. After equilibrating the sensor chip with HBS-P (10 mM HEPES pH 7.4, 150 mM NaCl, 0.005% Surfactant P20) at a flow rate of 5μl/min, the chip surface was activated with a 7 min pulse of 50 mM N-hydroxysuccinimide/200 mM N-ethyl-N′-(dimethylaminopropyl)-carbodiimide at a flow rate of 5 μl/min. 6xHis-SUMO-Jacob-Δ1-44 was immobilized on the surface of the sensor chip cell (CM5, Biacore AB, GE Healthcare) by injection of the ligand solution (20 μg/ml of protein in 10 mM Sodium acetate pH 4.0) for 7 min according to the manufacturer's instructions. Finally the excess of reactive groups on the chip surface was deactivated with a 7 min pulse of 1M ethanolamine hydrochloride (pH 8.5) at a flow rate of 5 μl/min. Binding studies including active GST-ERK1, inactive GST-ERK1 and GST controls were performed in the presence or absence of adenosine triphosphate (ATP, 30 μM). The purified proteins were diluted to the indicated concentrations in the continuous flow buffer HBS-P containing 7 mM Mg^{2+}. Each analytic run was performed at 20μl/min flow rate in the following order: First, one minute equilibration of the chip with the indicated analysis buffer was performed. Next, the analyte was injected in a 3 min pulse (association time) followed by a 3 minutes-pulse with analysis buffer alone (dissociation time). Individual runs were completed with the regeneration of the chip matrix using a 2 min-pulse of 50 mM NaOH at a flow rate of 5μl/min and a terminating 5 min pulse with flow buffer in order to equilibrate the chip surface again.

Hippocampal Slice Preparation, Electrophysiology, and Isolation of Nuclei from CA1 Region

Hippocampi from 21d-old male Wistar rats were cut using a vibratome (LeicaVT1000S, Nussloch, Germany) into 350 μm thick slices as described previously (Karpova et al., 2006; Behnisch et al., 2011) and incubated for 2h in carbogenated artificial cerebrospinal fluid (ACSF, containing in mM: 110 NaCl, 5 KCl, 2.5 $CaCl_2 \cdot 2H2O$, 1.5 $MgSO_4 \cdot 7H_2O$, 1.24 KH_2PO_4, 10 glucose, 27.4 $NaHCO_3$, pH 7.3) at 32°C. Field excitatory postsynaptic potentials (fEPSPs) were evoked by stimulation of Schaffer-collateral fibers with biphasic rectangular current pulses (200 μs/polarity) in a range of 3-4V through ACSF filled glass pipettes (0.5 MOhm). fESPSs were recorded using ACSF filled pipettes and amplified by an AxonClamp 200B amplifier (Axon, US) and digitized at a sample frequency of 10 kHz by Digidata 1400plus AD/DA converter (Axon, USA). Stimulation strength was adjusted to 40% of the maximum fEPSP-slope values. Responses to test stimuli were measured every minute throughout the experiment. LTP was induced by tetanization consisting of three 1 s trains at 100 Hz (Cai et al., 2010) every 5 min. 30 μM bicuculline were washed-in 2 min before tetanization and wash-out immediately after last tetanization to increase the field of stimulation within CA1 region. Slices were shock frozen 2 min or 30 min after induction of LTP and underwent dissection of CA1 regions in 4C° TBS containing protease inhibitors (Complete, ROCHE) and phosphatase inhibitors (Phosphostop, ROCHE). For each experiment (n = 5 for 2 min LTP and n = 6 for 30 min LTP) five potentiated and five control slices from the same experimental preparation were pooled together, homogenized and underwent nuclear isolation guided by a modified protocol provided in "CelLytic NuCLEAR Extraction Kit" (Sigma). Briefly, 5 dissected CA1 regions were homogenized in 50 μl of hypotonic buffer containing 10 mM HEPES, 1.5 mM MgCl2, 10 mM KCl, pH 7.9, with protease and phosphatase inhibitors. 10 μl of homogenate were taken as input for homogenate fraction. The progression of nuclear extraction was microscopically controlled in 2 μl of homogenate. At the time point when swelling of cells occurred and clear nuclei could be detected (usually 5-7 min), the homogenate was centrifuged for 1 min at 11.000 x g. The pellet fraction was resuspended in 40 μl of lysis buffer and enrichment of nuclei was controlled again under the microscope. Thereafter homogenate and nuclear fractions were solubilized in 4xSDS loading dye, total protein concentration was measured and 30 μg of each sample were subjected to SDS-PAGE with subsequent immunoblotting for pS180-Jacob. NeuN and β-actin were used as loading controls for homogenate and nuclear fraction respectively and normalization for loading was included into quantification of pJacob IR.

Whole-Cell Voltage-Clamp Recording of mEPSCs

Miniature excitatory postsynaptic currents (mEPSCs) of hippocampal primary neurons at DIV10-16 were recorded under whole-cell voltage-clamp conditions using 3-5 MOhm pipettes filled with an "intracellular" solution containing (in mM): Cs-methanosulfonate 110, NaCl 5, EGTA-acid 0.5, HEPES 10, ATP Na_2 4, GTP Na_2 0.4, phosphocreatine-Na_2 10, pH 7.25 (290 mOsm). To block spontaneous action potential generation and γ-aminobutyric acid type A receptors 500 nM TTX and 20 μM bicuculline were added to the extracellular solution that contained (in mM): NaCl 125, KCl 5, $CaCl_2$ 2, $MgCl_2$ 1 HEPES 10, glucose 10, pH7.30 (310 mOsm). Neurons on a coverslip were transferred to RC25 recording chamber (Warner, US) mounted on a Nikon Eclipse FN1 microscope equipped with 40x 0.80NA water dipping objective and FITC filter cube and were constantly perfused with recording medium at a rate of 1 ml/ min at room temperature. mEPSCs were recorded by a Multiclamp 200B (Axoclamp) amplifier and digitalized with Digidata 1440 and acquired by Clampex 10.2 (Axoclamp, US) software. Membrane potential was held at −70 mV and currents were processed through 1 kHz low-pass and 0.1 Hz high-pass filters. Up to 500 mEPSCs were collected over 3 min. Continuous recording of current traces was followed by off-line analysis of mEPSC parameters using Minianalysis 6 software. Only whole-cell

voltage-clamp recordings from cells with a membrane resistance of 100 to 300 MOhm and holding current of about 200 nA were included in the analysis.

Quantitative Real-Time PCR

Cortical primary neurons were infected with ΔMyr-Jacob-GFP, ΔMyr-Jacob-S180A-GFP, ΔMyr-Jacob-S180D-GFP or GFP alone using SFV at DIV18. Six hours after infection cells were lysed and total RNA was extracted and purified with Oligotex mRNA Mini Kit (QIAGEN GmbH, Hilden, Germany) according to the manufacturer's instructions. The mRNA level of BDNF and Arc/Arg3.1 were analyzed by quantitative real-time PCR system with pre-made TaqMan gene expression assays (Applied Biosystems/Life Technologies GmbH, Darmstadt, Germany) as described in the manufacturers protocol. The relative amounts of mRNA for BDNF (Assay ID Rn02531967_s1) and Arc/Arg3.1 (Assay ID Rn00571208_g1) were normalized to those of a Hprt1 (Assay ID Rn01527840_m1) control and relative comparisons were made to the GFP control group.

In Vitro Kinase Assay

For in vitro protein kinase assays bacterially produced purified MBP-Jacob-1-228 (rat sequence) or 6xHis-SUMO-Jacob-Δ1-44 (45-532, rat sequence) or 6xHis-SUMO-Jacob-Δ1-44 (45-532, mouse sequence) and recombinant active or inactive ERK1 (Proteinkinase.de, Kassel, Germany) were incubated in the presence of 30 μM of Mg^{2+}-ATP (Sigma-Aldrich, Taufkirchen, Germany) for 10, 20 and 30 min at 30°C (10 μM of fresh Mg^{2+}-ATP was added every 10 min) in phosphorylation buffer containing 50 mM Tris-HCl (pH 7.5), 150 mM $NaCl_2$, 1 mM EGTA, 1 mM EDTA, 10 mM $MgCl_2$ and 1 mM DTT. Reactions were terminated by addition of SDS sample buffer or by freezing the samples at −80°C. The efficiency of Jacob phosphorylation at S180 of the rat protein was checked by immunoblotting with pS180-Jacob antibody and both proteins (mouse and rat) were subjected to Matrix-assisted laser desorption/ionization-mass spectrometry.

Statistical Analysis

Comparison of Jacob immunofluorescence in synaptic stimulation experiments was performed with SPSS 11.5 and Statistica 6.0 using ANOVA followed by post-hoc Bonferroni tests. Statistical analysis of quantitative immunoblotting was performed using non-parametrical Mann-Whitney U-Test. t test (non-uniform variance) was employed for comparisons of mEPSC amplitude and frequency values in Jacob-S180A-GFP, Jacob-S180D-GFP and GFP expressing neurons. The accepted two-tailed alpha-error for statistical group comparison was $p \leq 0.05$.

SUPPLEMENTAL REFERENCES

Bekkers, J.M., and Stevens, C.F. (1989). NMDA and non-NMDA receptors are co-localized at individual excitatory synapses in cultured rat hippocampus. Nature *341*, 230–233.

Cai, F., Frey, J.U., Sanna, P.P., and Behnisch, T. (2010). Protein degradation by the proteasome is required for synaptic tagging and the heterosynaptic stabilization of hippocampal late-phase long-term potentiation. Neuroscience *169*, 1520–1526.

Chan, S.O., Runko, E., Anyane-Yeboa, K., Ko, L., and Chiu, F.C. (1998). Calcium ionophore-induced degradation of neurofilament and cell death in MSN neuroblastoma cells. Neurochem. Res. *23*, 393–400.

Cheung, P.C., Campbell, D.G., Nebreda, A.R., and Cohen, P. (2003). Feedback control of the protein kinase TAK1 by SAPK2a/p38alpha. EMBO J. *22*, 5793–5805.

Corbalan-Garcia, S., Yang, S.S., Degenhardt, K.R., and Bar-Sagi, D. (1996). Identification of the mitogen-activated protein kinase phosphorylation sites on human Sos1 that regulate interaction with Grb2. Mol. Cell. Biol. *16*, 5674–5682.

Davis, R.J. (1993). The mitogen-activated protein kinase signal transduction pathway. J. Biol. Chem. *268*, 14553–14556.

Fantz, D.A., Jacobs, D., Glossip, D., and Kornfeld, K. (2001). Docking sites on substrate proteins direct extracellular signal-regulated kinase to phosphorylate specific residues. J. Biol. Chem. *276*, 27256–27265.

Gietz, R.D., and Woods, R.A. (2002). Transformation of yeast by lithium acetate/single-stranded carrier DNA/polyethylene glycol method. Methods Enzymol. *350*, 87–96.

Hara, D., Fukuchi, M., Miyashita, T., Tabuchi, A., Takasaki, I., Naruse, Y., Mori, N., Kondo, T., and Tsuda, M. (2009). Remote control of activity-dependent BDNF gene promoter-I transcription mediated by REST/NRSF. Biochem. Biophys. Res. Commun. *384*, 506–511.

Ho, D.T., Bardwell, A.J., Abdollahi, M., and Bardwell, L. (2003). A docking site in MKK4 mediates high affinity binding to JNK MAPKs and competes with similar docking sites in JNK substrates. J. Biol. Chem. *278*, 32662–32672.

Hradsky, J., Raghuram, V., Reddy, P.P., Navarro, G., Hupe, M., Casado, V., McCormick, P.J., Sharma, Y., Kreutz, M.R., and Mikhaylova, M. (2011). Post-translational membrane insertion of tail-anchored transmembrane EF-hand Ca^{2+} sensor calneurons requires the TRC40/Asna1 protein chaperone. J. Biol. Chem. *286*, 36762–36776.

Jacobs, D., Glossip, D., Xing, H., Muslin, A.J., and Kornfeld, K. (1999). Multiple docking sites on substrate proteins form a modular system that mediates recognition by ERK MAP kinase. Genes Dev. *13*, 163–175.

Kapitein, L.C., Schlager, M.A., Kuijpers, M., Wulf, P.S., van Spronsen, M., MacKintosh, F.C., and Hoogenraad, C.C. (2010). Mixed microtubules steer dynein-driven cargo transport into dendrites. Curr. Biol. *20*, 290–299.

Karpova, A., Mikhaylova, M., Thomas, U., Knöpfel, T., and Behnisch, T. (2006). Involvement of protein synthesis and degradation in long-term potentiation of Schaffer collateral CA1 synapses. J. Neurosci. *26*, 4949–4955.

Lu, W., Man, H., Ju, W., Trimble, W.S., MacDonald, J.F., and Wang, Y.T. (2001). Activation of synaptic NMDA receptors induces membrane insertion of new AMPA receptors and LTP in cultured hippocampal neurons. Neuron *29*, 243–254.

Mansour, S.J., Matten, W.T., Hermann, A.S., Candia, J.M., Rong, S., Fukasawa, K., Vande Woude, G.F., and Ahn, N.G. (1994). Transformation of mammalian cells by constitutively active MAP kinase kinase. Science *265*, 966–970.

Pearson, G., Robinson, F., Beers Gibson, T., Xu, B.E., Karandikar, M., Berman, K., and Cobb, M.H. (2001). Mitogen-activated protein (MAP) kinase pathways: regulation and physiological functions. Endocr. Rev. *22*, 153–183.

Reynolds, C.H., Betts, J.C., Blackstock, W.P., Nebreda, A.R., and Anderton, B.H. (2000). Phosphorylation sites on tau identified by nanoelectrospray mass spectrometry: differences in vitro between the mitogen-activated protein kinases ERK2, c-Jun N-terminal kinase and P38, and glycogen synthase kinase-3beta. J. Neurochem. *74*, 1587–1595.

Seidenbecher, C.I., Langnaese, K., Sanmartí-Vila, L., Boeckers, T.M., Smalla, K.H., Sabel, B.A., Garner, C.C., Gundelfinger, E.D., and Kreutz, M.R. (1998). Caldendrin, a novel neuronal calcium-binding protein confined to the somato-dendritic compartment. J. Biol. Chem. *273*, 21324–21331.

Shevchenko, A., Wilm, M., Vorm, O., and Mann, M. (1996). Mass spectrometric sequencing of proteins silver-stained polyacrylamide gels. Anal. Chem. *68*, 850–858.

Smalla, K.H., Seidenbecher, C.I., Tischmeyer, W., Schicknick, H., Wyneken, U., Böckers, T.M., Gundelfinger, E.D., and Kreutz, M.R. (2003). Kainate-induced epileptic seizures induce a recruitment of caldendrin to the postsynaptic density in rat brain. Brain Res. Mol. Brain Res. *116*, 159–162.

Tsuriel, S., Geva, R., Zamorano, P., Dresbach, T., Boeckers, T., Gundelfinger, E.D., Garner, C.C., and Ziv, N.E. (2006). Local sharing as a predominant determinant of synaptic matrix molecular dynamics. PLoS Biol. *4*, e271.

Yang, S.H., Yates, P.R., Whitmarsh, A.J., Davis, R.J., and Sharrocks, A.D. (1998). The Elk-1 ETS-domain transcription factor contains a mitogen-activated protein kinase targeting motif. Mol. Cell. Biol. *18*, 710–720.

Yung, Y., Yao, Z., Aebersold, D.M., Hanoch, T., and Seger, R. (2001). Altered regulation of ERK1b by MEK1 and PTP-SL and modified Elk1 phosphorylation by ERK1b are caused by abrogation of the regulatory C-terminal sequence of ERKs. J. Biol. Chem. *276*, 35280–35289.

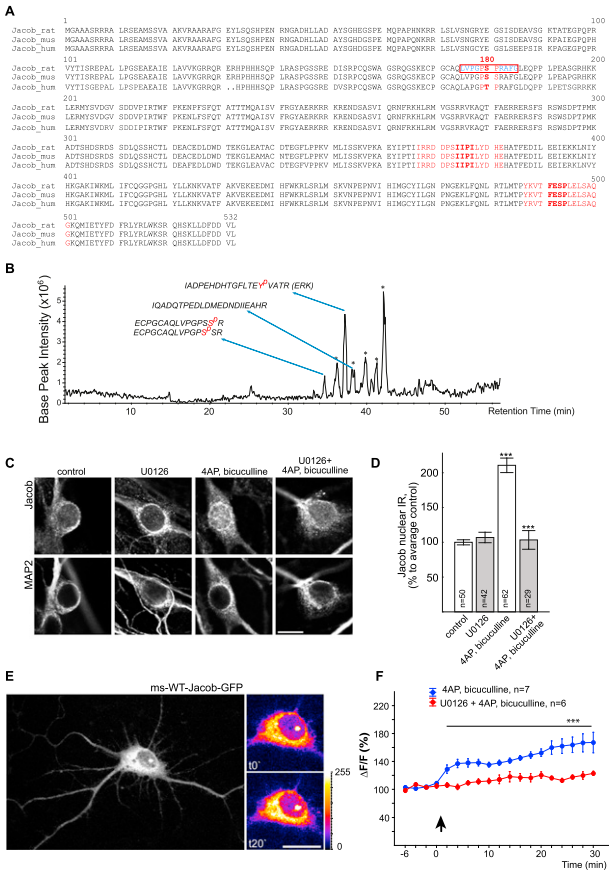

Figure S1. Jacob Is Phosphorylated by ERK1/2 at S180 in Rat and Mouse, Related to Figures 1 and 2

(A) S180 is a non-canonical ERK-phosphorylation site in human (Gene ID:26012), mouse (Gene ID: 56876) and rat Jacob (Gene ID: 117536) with a Pro-Gly-Pro-Ser/Thr-Pro motif instead of the classical Pro-X-Ser-Pro motif. Moreover, despite the high conservation between different species the mouse sequence exhibits a major deviation with a serine instead of proline at position 181 which would transform this site into a high-scoring PKC site. Although the mouse does not correspond to the minimal consensus sequence (Ser/Thr-Pro) for phosphorylation by MAP kinases (Davis, 1993), it is important to note that the Ser/Thr-Pro motif is not a requirement for MAP kinase phosphorylation. Previous studies have identified noncanonical substrates of MAP kinases, including the ERK sites Ser1132-Ala and Ser1197-Ile in Sos1 (Corbalan-Garcia et al., 1996), the p38 MAPK site Ser423-Ala in TAB1 (Cheung et al., 2003), the p38 MAPK sites Ser185-Gly, Thr245-Ala, Ser305-Val, and Ser356-Leu in Tau (Reynolds et al., 2000), and the JNK site Ser356-Leu in Tau (Reynolds et al., 2000). The ERK binding sequence in Jacob (aa367-382) was identified by its similarity to the known binding motif (K/R1-2 –X1-6-L/I-X-L/I, Jacobs et al., 1999) in ERK substrates. It harbors an IIPI sequence (D-box) that is crucial for the interaction with the ERK1/2 DxxD motif (Pearson et al., 2001; Yang et al., 1998; Fantz et al., 2001; Ho et al., 2003). The second potential ERK1/2 docking site in Jacob (sequence aa487-501) contains an FxSP (aa491-494) motif that is similar to the well-known FxFP motif mediating the interaction of other substrates with ERK (Jacobs et al., 1999; Fantz et al., 2001). Red box indicates the peptide sequence used for immunization.

(B) Mouse Jacob is phosphorylated by ERK1/2 at S180 and S181. A 6xHis-SUMO-Jacob-Δ1-44 construct was cloned from mouse cDNA, and the protein was expressed in and purified from bacteria. 6xHis-SUMO-Jacob-Δ1-44 was phosphorylated by active ERK1 in vitro, digested with trypsin and resulting phosphopetides were enriched by TiO sphere affinity chromatography. Phosphorylated peptides are indicated in the base peak chromatogram. Asterisks denote base peaks, which are neither Jacob nor ERK derived single charged ions. Subsequent MALDI-TOF analysis revealed that in mouse both Ser180 and 181 are phosphorylated by ERK1.

(C and D) Like in rat hippocampal primary neurons, synaptic activity and subsequent activation of ERK1/2 are also required for the nuclear accumulation of endogenous Jacob in mouse primary cultures. Experiments were done at DIV18 in the presence of anisomycin (7.5 μM). Data are represented as mean +/− SEM. ***p < 0.001 as determined by Bonferroni corrected t tests. Scale bar is 20 μm.

(E and F) Further indirect proof that mouse Ser180 might also be an ERK phosphorylation site in vivo came from time-lapse imaging experiments when rat hippocampal neurons were transfected with the mouse wild-type Jacob construct (ms-WT-Jacob-GFP). ms-WT-Jacob-GFP translocates into the nucleus upon enhanced synaptic activity and this translocation is significantly attenuated by inhibition of the MEK-ERK pathway. E (left panel) depicts a confocal image of a rat hippocampal neuron expressing ms-WT-Jacob-GFP. Nuclear plane images shown in a gradient lookup table from neuronal somata before (t0′) and 20 min after (t20′) enhanced synaptic activity (E, right panel). Scale bar is 20 μm. (F) Quantitation of nuclear ms-WT-Jacob-GFP fluorescence intensities with (red circles) and without the MEK1/2 inhibitor U0126 (blue circles). Arrow indicates the time point for bath application of 50 μM bicuculline. In summary, several lines of independent evidence suggest that S180 is a non-canonical ERK-phosphorylation site of Jacob in human, mouse and rat. Data are represented as mean +/− SEM. ***p < 0.001 as determined by Bonferroni corrected t tests.

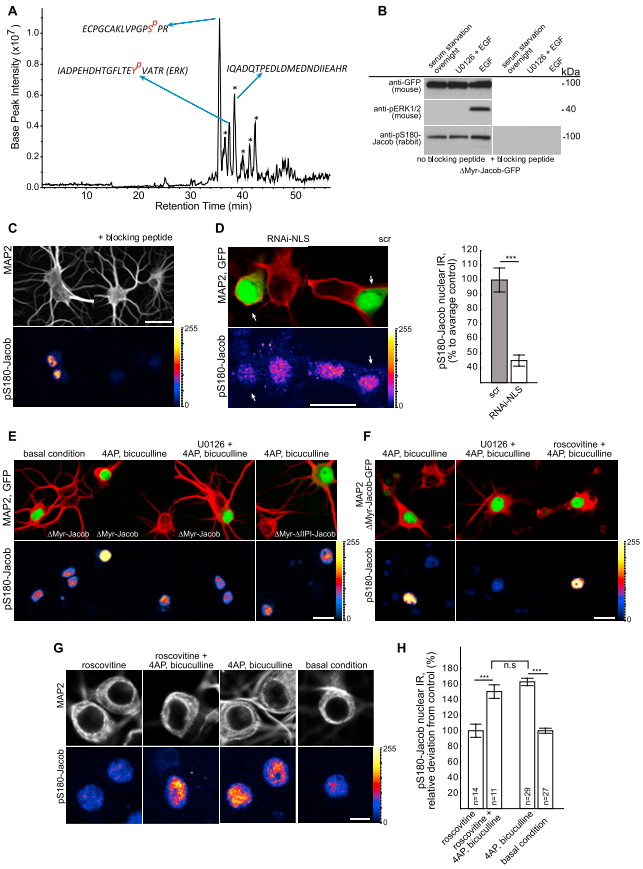

Figure S2. Jacob Is Phosphorylated at Ser180 In Vivo, Related to Figure 2

(A) ERK phosphorylates Jacob in 18DIV cortical primary neurons treated with 50 μM bicuculline. Nuclear extracts from WT-Jacob-GFP infected neurons were separated in duplicate by SDS-PAGE. One lane from each sample was processed for immunoblotting with GFP and pS180-Jacob antibody and second one was stained with commassie blue. Area corresponding to the band of WT-Jacob-GFP was cut out from the SDS gel and underwent InGel-digestion. Resulting peptides were subjected to a nano-reversed phase (C18)-HPLC online coupled to an ETDII iontrap mass spectrometer. MS/MS precursor selection was tuned for the preferential use of masses corresponding to a double charged (852.36 Da) putative ECPGCAQLVPGPSPPR Jacob peptide. Depicted is the mass spectrum at retention time 43.3 min including the 852.62 Da double charged base peak peptide which was selected as a precursor for two independent CID (collision induced dissociation) fragmentations. Both MS/MS experiments significantly revealed sequence identity of the selected precursor to the phosphorylated ECPGCAQLVPGPSpPR sequence of Jacob.

(B) Affinity-purified phospho-specific antibody detects phosphorylated ΔMyr-Jacob-GFP expressed in HEK293 cells. An increase in pS180-Jacob IR can be detected after stimulation of the MAPK pathway with EGF. This phosphorylation was sensitive to the MEK1/2 inhibitor U0126 (10 μM). Antibodies against active ERK1/2 were used to determine kinase activation level. The pS180-Jacob immunosignal was completely blocked by pre-incubation of the antibodies with a S180 phosphopeptide LVPGPSpPRAFG.

(C) pS180-Jacob immunostaining of rat hippocampal primary neurons could be blocked by pre-incubation of the antibodies with a S180 phosphopeptide LVPGPSpPRAFG.

(D) Nuclear Jacob knock down reduces pS180-Jacob immunoreactivity. Arrow indicates a cell that was transfected with the shRNA construct. Data are represented as mean +/− SEM. ***p < 0.001 as determined by t test.

(E) Increased nuclear pS180-Jacob IR was detected in hippocampal neurons expressing ΔMyr-Jacob-GFP following bath application of bicuculline. Inhibition of the MAPK pathway as well as disruption of the D-box in a deletion mutant (ΔMyr-ΔIIPI-Jacob) prevented phosphorylation of overexpressed ΔMyr-Jacob following enhanced synaptic activity.

(F) Pre-incubation of the cultures with the CdK5 inhibitor roscovitine did not prevent ΔMyr-Jacob-GFP phosphorylation following enhanced synaptic activity.

(G and H) The CdK5 inhibitor roscovitine has no effect on the phosphorylation of endogenous Jacob at Ser180. These experiments were part of those depicted in Figure 2D and the bar graphs in H depicting the control and enhanced activity condition are identical to those in Figure 2D. Data are represented as mean +/− SEM. ***p < 0.001 as determined by Bonferroni corrected t tests. Scale in C is 40 μm; Scale in D, E and F is 20 μm. Scale in G is 10 μm

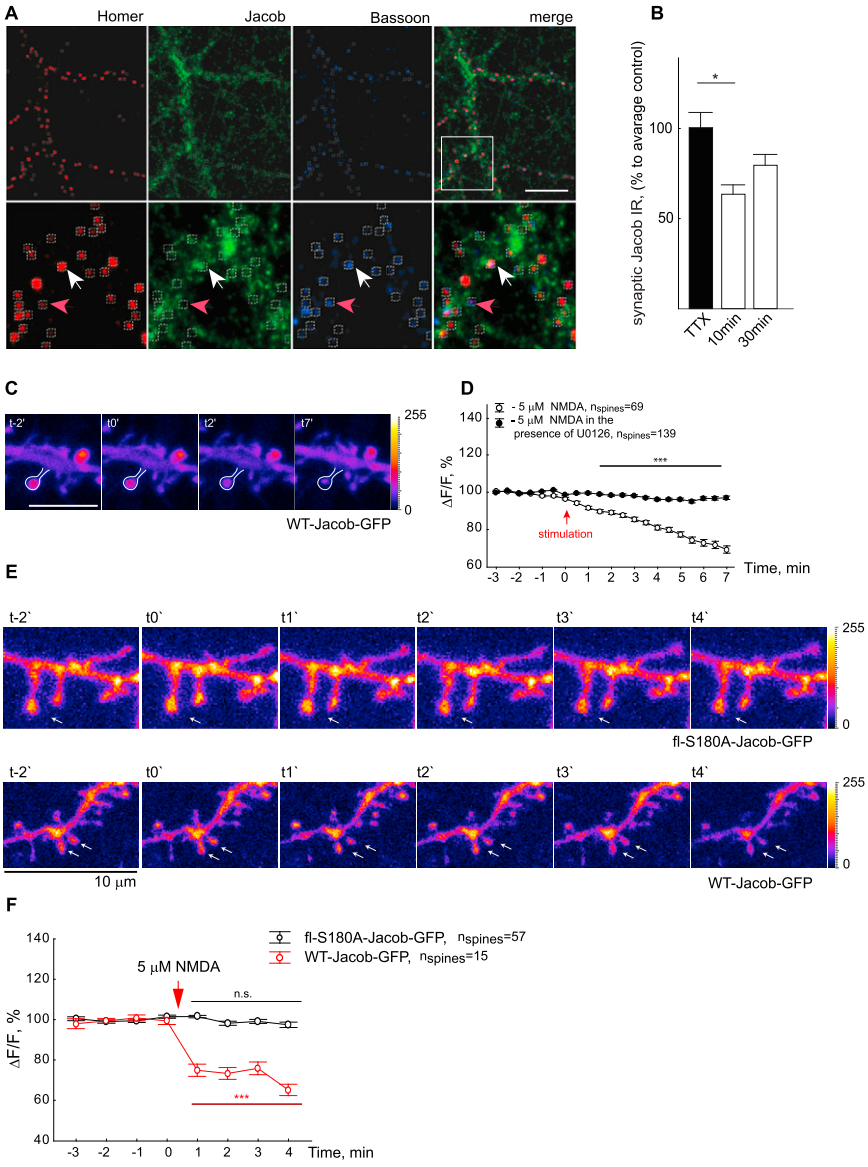

Figure S3. Enhanced Synaptic Activity Induces a Reduction in Synaptic Jacob Immunofluorescence, Related to Figure 3

(A) Representative image of DIV21 hippocampal neuron taken for quantification. Homer (red) and Bassoon (blue) staining was used to quantify excitatory synapses. Scale bar is 10 μm. The lower panel shows a zoomed in area where white arrows indicate a synapse positive for pre-, postsynaptic markers and Jacob, while red arrows point to synapses that lack Jacob or have very low Jacob levels. Dotted rendered white boxes indicate synapses that were included for analysis.

(B) Quantification of synaptic pan-Jacob as percent deviation from control (group treated with 1 μM of TTX for 30 min) upon treatment with 50μM bicuculline for 10 and 30 min. Data were obtained from 10 images per group. The mean value for each image was calculated from approximately 100 synapses. Bars represent mean values; error bars represent ± 1 standard error of the mean. *$p < 0.05$ as determined by t test.

(C and D) WT-Jacob-GFP but not the fl-S180A-Jacob-GFP rapidly dissociates from mature synapses upon activation of synaptic NMDARs. Hippocampal neurons were transfected at DIV23/28. Confocal average intensity images of a 10 μm dendritic segment before and after the indicated treatment are shown. Represented images were not corrected for bleaching. Data are represented as mean +/− SEM. ***$p < 0.001$ as determined by Bonferroni corrected t tests.

(E and F) WT-Jacob-GFP but not the fl-S180A-Jacob-GFP rapidly dissociates from mature synapses upon activation of synaptic NMDARs. Hippocampal neurons were transfected at DIV23/28. Confocal average intensity images of a 10 μm dendritic segment before and after the indicated treatment are shown. Represented images were not corrected for bleaching. Data are represented as mean +/− SEM. ***$p < 0.001$ as determined by Bonferroni corrected t tests.

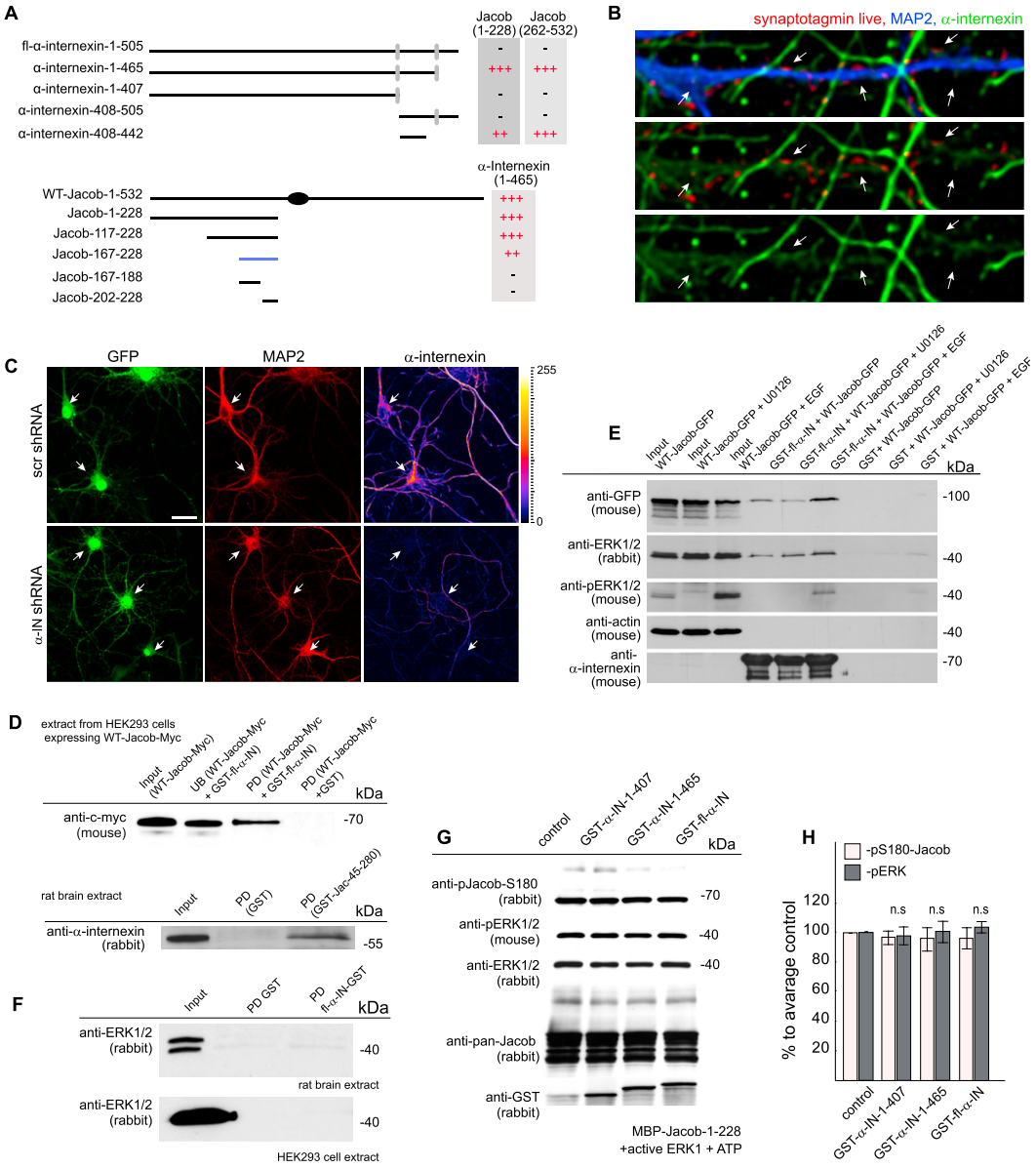

Figure S4. Jacob Is an α-Internexin Binding Partner, Related to Figure 4

(A) Mapping of the Jacob-α-Internexin interaction region using Matchmaker TM GAL4 Two Hybrid System. (+++) and (++) indicates strong and weak interactions, (-) indicates no interaction. The strength of interaction was evaluated based on the number of colonies growing in triple drop-out media; Grey boxes represent calpain cleavage sites. Black oval boxes represent the NLS.

(B) α-Internexin IR detected in dendrites and spines. Synaptotagmin antibodies labeled with Oyster 550 were added to the culturing medium 10 min prior to fixation in order to label active synapses. Depicted are confocal images from 23DIV hippocampal primary neurons acquired as Z-stacks.

(C) Depicted is the shRNA knock down of α-internexin in hippocampal primary neurons as detected with an Abcam ab_7259 antibody used in B and Figure S4B. Scale bar is 40 μm.

(D) The interaction between Jacob and α-internexin confirmed by pull down assays. Bacterially expressed GST-full-length-α-internexin fusion protein but not corresponding GST-control protein pulls down WT-Jacob-Myc from HEK239 cell extracts.

(E) Binding of heterologously expressed WT-Jacob-Myc from HEK239 cell extracts to GST-full-length α-internexin is modulated by MAPK activity. The interaction is stronger following stimulation of HEK239 cells with EGF and weaker after blocking MEK activity with the inhibitor U0126. Note that there is more ERK in the complex after EGF stimulation.

(F) GST-full-length α-internexin does neither pull down ERK1/2 from rat brain nor from HEK293 cell extracts.

(G and H) Binding of α-internexin does not compete with ERK-binding and nor does it prevent phosphorylation of Jacob by ERK in in vitro kinase assays. MBP-Jacob-1-228 fusion protein was phosphorylated in vitro in the presence of equimolar amounts of purified GST-α-internexin-1-407, GST-α-internexin-1-465 and GST-full-length-α-internexin. Data are represented as mean +/− SEM.

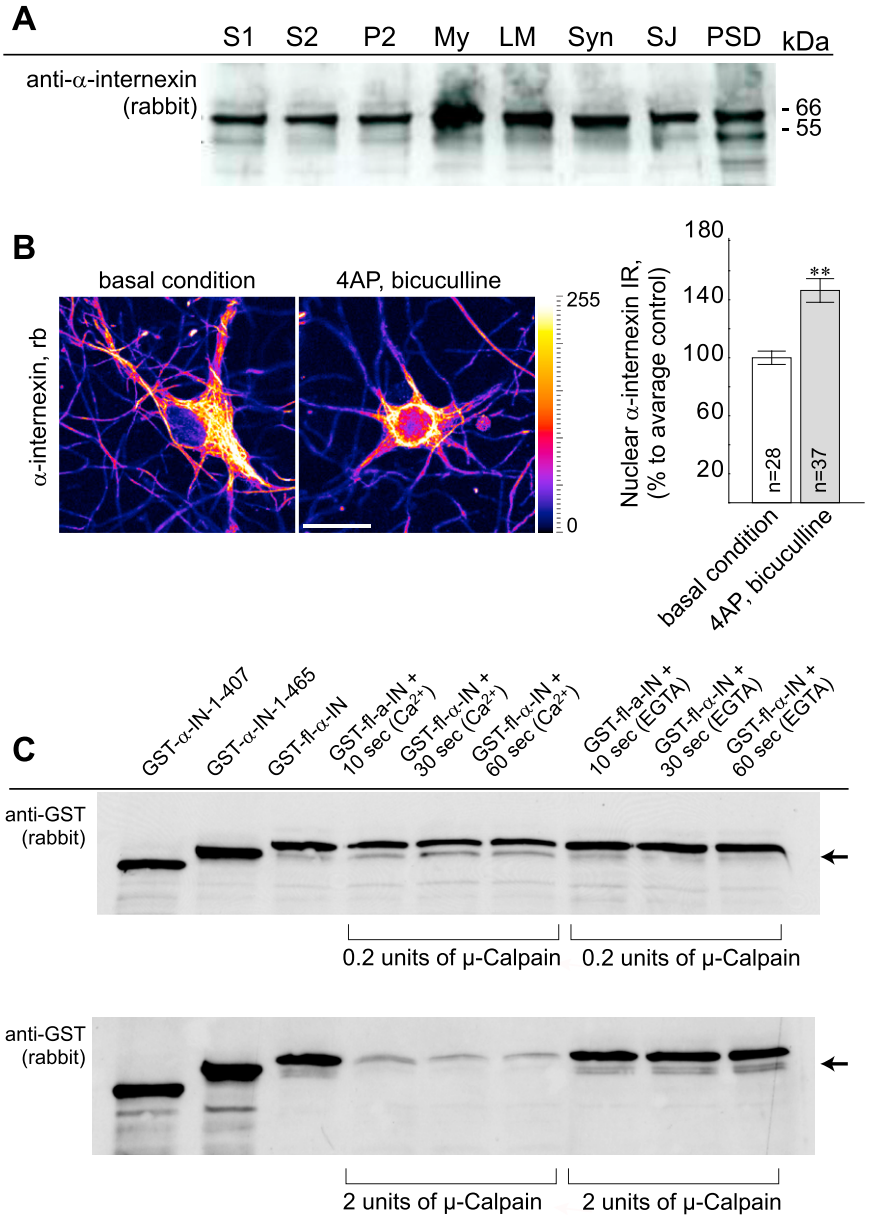

Figure S5. α-Internexin Is Present in the PSD and Is a Substrate of Calpain, Related to Figure 4

(A) α-internexin is present in soluble and insoluble protein fractions including the PSD. The fractions were obtained by differential centrifugation of homogenates of adult rat brain. 20 μg of protein was loaded in each lane. α-internexin was detected using a polyclonal rabbit antibody (Chemicon). (S1 - pre-cleaned homogenate after centrifugation; S2 – supernatant after centrifugation of S1 at 12.000 xg; P2 - crude membranes; My. - myelin fraction; LM-light membranes; Syn- synaptosomes; SJ - synaptic junctions; PSD - postsynaptic density fraction).

(B) α-internexin IR detected with an anti-α-internexin rabbit (Abcam) antibody increases in the nucleus in response to enhanced synaptic activity. Scale bar is 20 μm. Data are represented as mean +/− SEM. ***$p < 0.001$ as determined by Bonferroni corrected t tests. **$p < 0.01$ as determined by t test.

(C) α-internexin is cleaved by μ-Calpain in vitro. It has been reported previously that α-internexin is sensitive to Calpain mediated proteolysis, but neither the cleavage products nor the cleavage sites of α-internexin were identified (Chan et al., 1998). However, a prominent intermediate cleavage product is conspicuously present on Western blots from rat brain including the PSD fraction (see above). In analogy to vimentin (Perlson et al., 2005) we indeed found that recombinant α-internexin is rapidly degraded by Calpain and cleavage is sensitive to Ca^{2+}. Interestingly, the cleavage fragments generated from GST-fl-α-internexin would correspond to the size of GST-α-IN-1-465. These fragments bind to Jacob (see main text and Figure 4) and although their protective effect against phosphatase activity is considerably weaker than the full length protein, they might represent the endogenous binding partners for Jacob. Arrow indicates detection of the cleaved GST-α-internexin matching with the size of GFT-α-internexin-1-465.

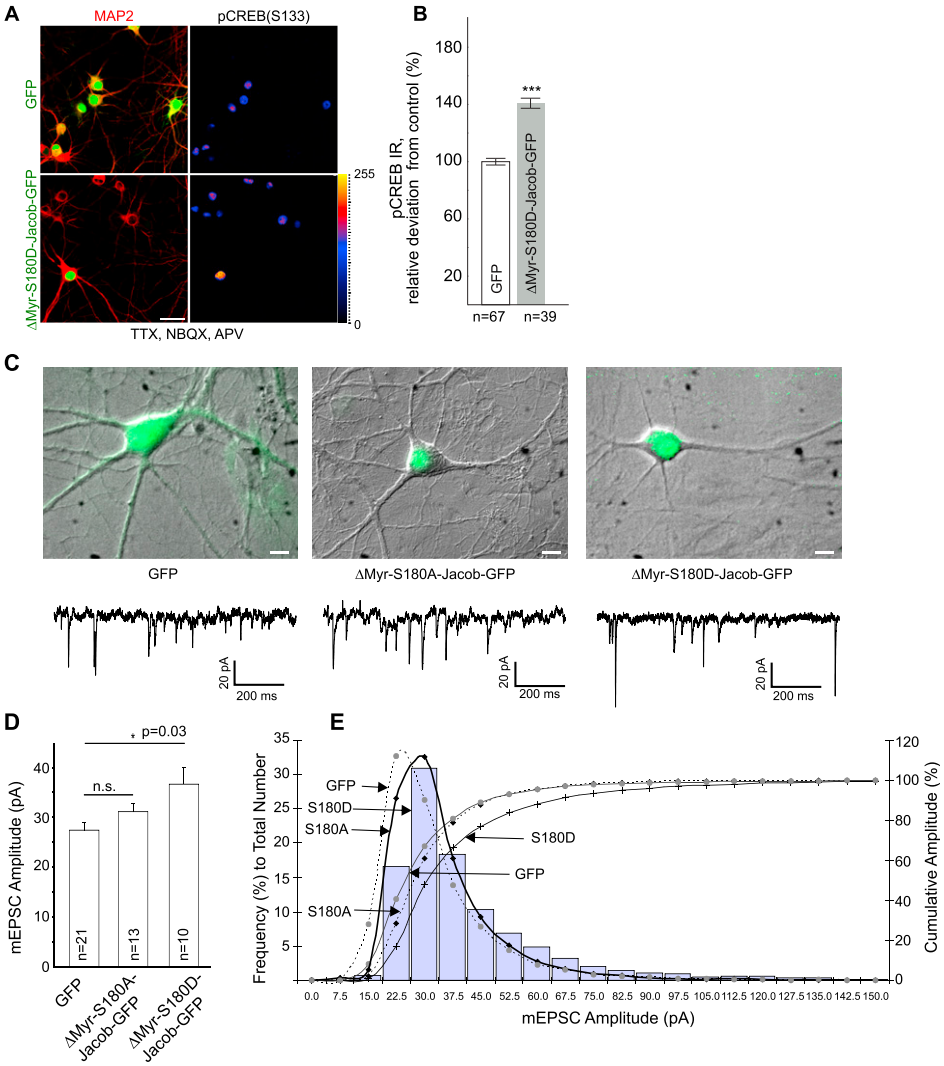

Figure S6. Nuclear Overexpression of Phosphomimetic ΔMyr-Jacob-S180D-GFP Increases CREB S133 Phosphorylation in the Absence of Synaptic Activity and Facilitates AMPA Receptor-Mediated Synaptic Transmission, Related to Figure 6

(A and B) Overexpression of nuclear phospho-mimetic Jacob (ΔMyr-S180D-Jacob-GFP) results in a significant increase in pCREB levels in silenced cultures. Hippocampal neurons were treated with TTX (1 μM), NBQX (10 μM) and APV (20 μM) for 24 hr. Six hours prior to fixation DIV17 neurons were infected with ΔMyr-S180D-Jacob-GFP or GFP using Semliki Forest virus particles. Scale bar is 10 μm in A. Data are represented as mean +/− SEM. ***$p < 0.001$ as determined by t test.

(C) Overlaid DIC (gray) and fluorescence (green) images of hippocampal neurons at DIV14 overexpressing GFP, ΔMyr-S180D-Jacob-GFP and ΔMyr-S180A-Jacob-GFP and corresponding representative traces of mEPSCs recorded at a holding potential of −70 mV 6-8h after transfection are depicted. Scale bar is 10 μm.

(D) Whole-cell voltage clamp recordings of mEPSCs at a holding potential of −70 mV. The bar diagram represents the mean+s.e.m of mEPSC amplitudes for different groups. Significant differences in means of mEPSC amplitudes between GFP and ΔMyr-S180D-Jacob-GFP overexpressing neurons were tested by t test. *$p \leq 0.05$.

(E) The diagram represents the frequency histogram (left *y* axis) and cumulative distribution (right *y* axis) of amplitudes of all mEPSCs collected from neurons expressing GFP, ΔJacob-S180A-GFP, ΔMyr-S180D-Jacob-GFP. The frequency of mEPSC amplitude distribution was normalized to the total number of mEPSCs of each group. The distribution of mEPSC amplitudes from ΔMyr-Jacob-S180D-GFP overexpressing neurons is depicted with vertical gray bars, ΔMyr-S180A-Jacob-GFP with a black line and black filled boxes and GFP with a gray dotted line and gray filled circles. The corresponding cumulative values are shown with black line and plus symbols, with black dotted line and black circles and with gray dotted line and gray circles for ΔMyr-S180D-Jacob-GFP, ΔMyr-S180A-Jacob-GFP and GFP respectively. The frequency histogram and cumulative diagram indicate a shift toward larger mEPSC amplitudes in Jacob-S180D-GFP overexpressing neurons in comparison to GFP control. Analysis of mEPSCs parameters from ΔMyr-Jacob-S180D-GFP overexpressing neurons revealed a mean mEPSC amplitude of 36 ± 3.4pA at a frequency of 13 ± 2.7Hz which were significantly different from GFP expressing cells (27 ± 1.5pA at a frequency of 5 ± 0.9Hz) indicating that nuclear overexpression of phospho-mimetic Jacob mutant most likely increases AMPA receptor mediated synaptic transmission.

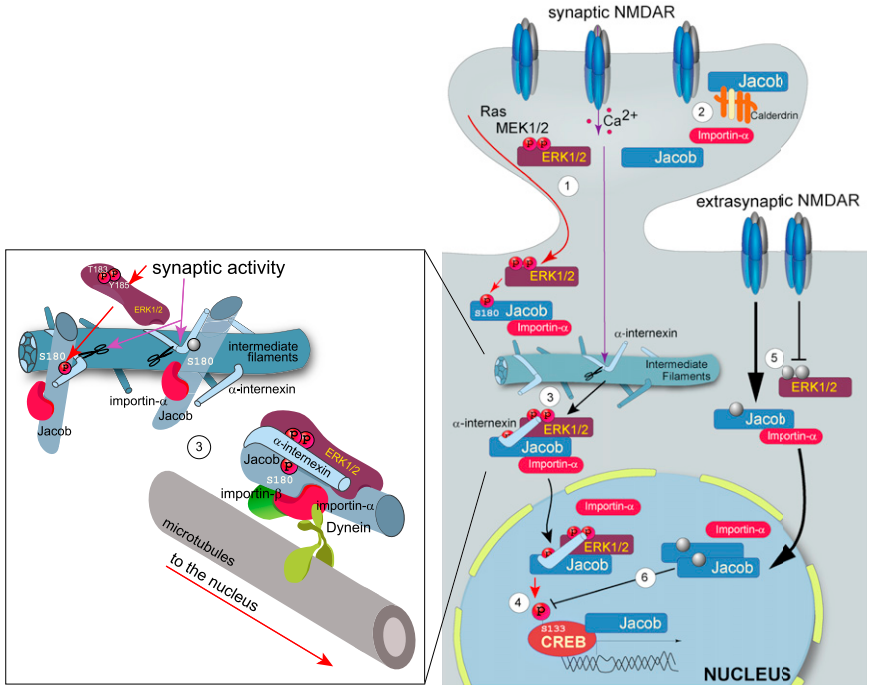

Figure S7. The Jacob Pathway Encodes the Synaptic or Extrasynaptic Localization of Activated NMDAR, Related to Figure 1

(1) Synaptic NMDAR activity leads to activation of ERK1/2 and subsequent binding and phosphorylation of Jacobs Ser180 at synaptic sites which in turn is a prerequisite for Jacob to leave the synapse. (2) A fraction of pJacob might be kept at the synapse via an interaction with the synaptic Ca^{2+}-sensor Caldendrin, which competes with importin-α for Jacob binding in a Ca^{2+}-dependent manner (Dieterich et al., 2008). This competition might either be necessary to keep the protein in spines for phosphorylation by ERK and the subsequent assembly of a transport complex or it might limit the amount of protein available for synapse-to-nucleus communication. In combination with the translation of the dendritic Jacob mRNA, that can replenish the local Jacob pool (Kindler et al., 2009), this will provide a dynamic equilibrium of synaptically localized and mobile Jacob (Figure S7). (3) Synaptic activity and subsequent increase in intracellular Ca^{2+} concentrations activate calpain, which in turn cleaves α-internexin and Jacob. This could result in the formation of a soluble α-internexin fragment. Soluble α-internexin interacts with the pJacob/pERK complex and protects pJacob and pERK against dephosphorylation during long-distance transport. The interaction of Jacob with α-internexin is stronger in case of Ser180 phosphorylation and α-internexin binding does neither compete with Jacob/ERK-binding nor does it prevent phosphorylation of Jacob by ERK. The pERK-internexin-pJacob complex can be linked via importin-α to a dynein motor, which might mediate active transport of the complex along microtubuli. (4) The presence of pJacob in the nucleus correlates with enhanced CREB phosphorylation, increased expression of plasticity-related genes and an increase in mEPSC amplitude indicative for enhanced synaptic strength. (5) The nuclear translocation of Jacob after extrasynaptic NMDAR activation does not require ERK activity and Jacob is not phosphorylated prior to nuclear import. (6) The nuclear accumulation of non-phosphorylated Jacob results in CREB shut-off and is followed by a series of deteriorative events in terms of synaptic and dendritic integrity and causes subsequent cell death.